Università degli Studi di Padova

Dipartimento di Ingegneria dell'Informazione

Master Thesis in Control System Engineering

Power System Identification and Online Tuning of Power System Stabilizers

Master Candidate

Diego Cifelli

Student ID 2019117

Supervisor

Prof. Ruggero Carli

University of Padua

Co-supervisor

Prof. Luca Schenato

University of Padua

Dott. Catalin Gavriluta

AIT Austrian Institute Of Technology

Date

05/12/2022

Academic Year

2022/2023

To my family
and friends

Abstract

In this master thesis a framework for the identification of a low-order model of the electric power system and the online tuning of Power System Stabilizers (PSSs) is presented. The goal is to improve the damping of power oscillations, i.e., active power oscillations that emerge due to the interaction between the synchronous generators present in a power system. If these oscillations are not dampened through proper control action, they can become problematic, increasing the possibility of a total power system collapse. The most used controller to damp these oscillations is the PSS, which is installed in some of the large electric generators present in the grid. The standard approach in the field is to deploy these controllers following a *"set and forget"* approach, meaning that the controllers are tuned once during the initial power plant commissioning, and almost never re-tuned during the lifetime of the generator. However, in modern power systems the configuration of the system is not static, but continuously changes over time, for example due to the installation of new power sources or due to changes in grid topology. Even during normal operation there may be large variability, for example due to different power generation profiles yielded by renewable sources. Hence, in order to address these issues, the PSSs should be ideally adapted to the new configuration in order to guarantee proper oscillation damping performance. To solve this problem, we propose a solution based on a system identification procedure to first identify a low-order linear system of the power system. Then we use this estimated model to tune the PSSs on the current configuration. To validate the proposed method, we perform simulations in Matlab and in Hypersim, a real-time power system simulator.

AIT Austrian Institute of Technology is Austria's largest Research and Technology Organisation (RTO) and an international key player in many of the research areas it covers.

This thesis was performed in collaboration with the Center for Energy inside the Electrical Energy Systems competence unit. [1]

Contents

1 Introduction

In this introductory chapter, we begin with a small introduction to the electricity grid. Next, we present the problem we wish to solve in this work and the solution we propose. We continue with the state of the art and conclude with our contribution.

1.1 Electric Power System

The electric power system is one of the most extensive and complex systems developed by humans. Its purpose is the production of the electric power that is needed for our life and transport it from the power plant to the end consumers. The power system can be divided into three areas: generation, transmission, and distribution. Historically, the generation is composed of a relatively small number of large power plants connected to the transmission grid. They are usually hydro or thermal power plants where the mechanical energy generated by a turbine is converted into electrical power. This conversion is carried out by synchronous generators, which are discussed in details in the next chapters. These synchronous generators feed the produced electricity into the transmission system via a step-up transformer to increase the voltage to the transmission voltage reference.
In recent years, with the development of renewable energy sources and their installation, the power system is becoming more and more complex and the control of the entire system more challenging.

The transmission network connects the power plants and transmits the generated power to the distribution grid. The connection of the generation units through the transmission grid makes the system highly coupled and complex, in which each component influences the rest of the components. So the transmission grid covers a crucial role in the integrity of the entire system and appropriate controls are implemented to ensure the stability of the system. Finally, the distribution brings power from the transmission to the consumers.

We will work on the generation and transmission level, meanwhile, the distribution grid is substituted with loads, which include all the consumers connected to a particular node of the transmission grid.

1.2 Problem statement

Low-frequency power oscillations are active power oscillations that can appear in a power system. If they are not correctly controlled and damped, they can diverge and even cause the collapse of the system. They are intrinsic in the system dynamics, but there are some factors that can increase their strength, e.g. long or highly loaded tie-line between different areas of the system, generators with high power, and also fast excitation systems used to control the voltage in the grid.

In [2], [3], [4] some analysis of this type of events that occurred in the real power system are reported. In the next years, with the large integration of renewable energy sources and the expansion of the grids, the power system could be more susceptible to this type of events [5].

The low-frequency oscillation can be divided into different categories: local oscillation, in which one machine oscillates against the rest of the system; inter-area oscillation, in which two machines from the same area oscillate one against the other; intra-area oscillation, in which a group of generators in an area of the system oscillates against a group from another area.

We think the combination of oscillation surveillance by analyzing the ambient data collected from PMU [6] devices spread in the power grid [7] and the online adaptation of the controllers can help to avoid unstable oscillations. In this work, we focus on the second part of the solution, mainly how to adapt the controllers to evolving power system configurations. We consider a specific type of controller, i.e. the power system stabilizer, which is one of the most used controllers for oscillation damping purposes. In particular, we have a fixed control structure, and we want to re-tune the parameters to always guarantee the required performance. We use a model-free approach in which a low-order linear model of the power system is identified from the data. This model is used to design the new parameters of the PSS.

1.3 State of the Art

In the recent years, with the increasing deployment of PMUs, different methods for the identification of the oscillations in power system have been presented. Different type of data can be used for the identification, e.g., ambient data - collected during the normal operation of the system and caused by the load variations, ring-down data

- collected after a fault that excite the system, probing data - in which the system is excited through injecting probing signals in the input of some controllers.

Each category has its advantages and disadvantages. Ambient data can be collected in any moment but their spectrum is typically not "rich" enough for a correct identification. Instead, ring-down data are usually richer of information but can be collected only after an event. Finally, probing data can be collected in any moment and are also rich of information, since one has the freedom to the design the probing signal. Instead, the main disadvantage is that one needs to perturb the system and this is not always possible.

Reference [8] is the first study on oscillation identification in which Prony's method is used to identify the frequency and damping factor of low-frequency oscillations. It shows good results, but the method is highly susceptible to noise [9]. From this initial study, different other methods has been applied, refining the Prony method [10], or using other techniques as fast Fourier transform [11], matrix pencil method [12], ARMAX transfer function model identification [13], subspace state-space and stochastic subspace methods [14]. In all these works, both ambient and ring-down data are used for the identification.
These methods are based on the assumption that the power system can be linearized around the operating point and the estimation of a linear model can be used for correct oscillations identification. Indeed, [15] shows that a linear system is a good approximation of the non-linear power system also for large disturbances.

Moreover, in general ambient and ring-down data can be used for oscillations identification but not for deriving an input-output relation that can be used to design the controller in the system. For this reason, the probing data-based method is the most suitable for the online re-tuning of PSSs.

In [16], a review of different methods based on probing signals for different tasks is presented. They are used not only for system identification but also for other scopes, like inertia estimation [17] and impedance characterization [18]. Probing data are used for oscillation identification in [19], [20], but only a few works [21],[22], [23] analyze the problem of identifying a model of the system that can be used to design a controller, especially for PSS re-tuning.

A similar approach to the one proposed by us in this thesis has been presented in [24]. They use an ARMAX transfer function model for the power system identification and a method based on linear matrix inequalities for tuning the PSS's parameters. The developments introduced by our work are presented in the next section.

1.4 Contributions

In the first part of the thesis, we compare different system identification methods to find the one that gives the best accuracy for the studied problem. In particular, we

consider both polynomial transfer function models (including also ARMAX used in [24]) and state-space models. Different identification algorithms are implemented and their performance compared. In the second part, we present a method to design the PSSs parameters given the identified model and we validate both the identification and the controller design with real-time simulation. Compared to [24], we find a better identification method than the ARMAX model method and we validate the techniques on larger and more complex power systems.

2

Synchronous generators: model and control

In this chapter, we present the synchronous generator and its control system. Moreover, we discuss the modal analysis that can be used to understand the oscillatory behaviour of a power system.

2.1 Synchronous generator

The main component of a power system is the synchronous generator (SG), which is the device that generates the electric power. SG transforms the mechanical power generated by a turbine into electric power that is injected into the electric grid. It is composed of a stator, the fixed part of the machine, and a rotor, the moving part connected to the turbine shaft. In the rotor, we find the excitation system that generates a rotating electromagnetic field that induces an electromotive force in the three-phase stator winding.

The model of a SG is fairly complex, all the details can be find in [25]. In general, the complete model is made of nine non-linear differential equations and three algebraic equations that relate the stator and rotor fluxes with the terminal voltage, currents, rotor angle, and speed of the machine.

If we consider an entire power system involving multiple SGs, transformers, the network of lines and cables as well as other devices that may be present, the overall system is highly dimensional and complex. Usually all the variables in a power system are expressed in the Per-Unit system (p.u.) in which the variables are expressed as a fraction of a base quantity. In this way, all the variables lie in the same range and it is simpler doing the calculations when transformers are involved with different voltage level, at the two sides.

The rotor speed, the electric power and the output voltage are usually regulated by

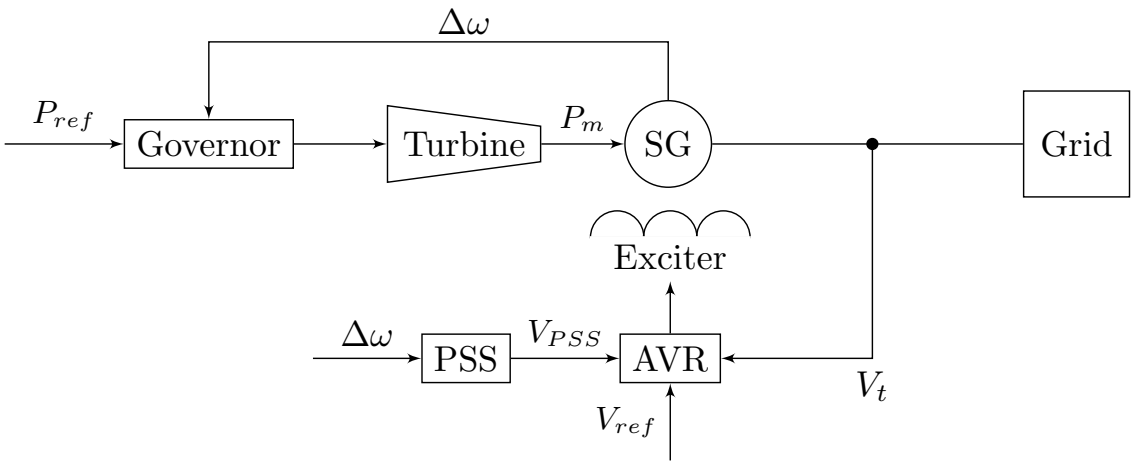

Figure 2.1: Synchronous generator control diagram

proper controllers, briefly described in the next section. The control diagram of a SG is shown in Fig. 2.1.

2.1.1 Turbine and Turbine Governor

In general, the synchronous generator is driven by either steam turbines, gas turbines or hydro turbines. The turbine is equipped with a governor system to regulate the output mechanical torque and operate at the required power. The governor consists of a droop control, a simple proportional control that regulates the output power based on the speed deviation of the generator. In particular, if the speed is less than the nominal one, the governor will increase the generating power to balance the speed deviation. Contrary, if the speed is larger than the nominal one, the governor will decrease the generating power. In general, different models exist for the turbine and the governor,a comprehensive list can be found in [26]. We report here the IEEE TGOV1 model, shown in Fig. 2.2, that we used in the simulations. It is a simplified model of a steam turbine, where R is the droop coefficient, T_1 is the time constant of the steam control valve, T_2 and T_3 model the motion of the steam through the reheater and turbine stages, D_t is the possible mechanical damping of the turbine and V_{min}, V_{max} represent the saturation of the steam valve. The power reference is P_{ref}, meanwhile P_m is the output mechanical power of the turbine that will be transformed in electrical power by the synchronous machine.

2.1.2 Excitation circuit and Automatic Voltage Regulator

The excitation circuit is responsible for generating the electromagnetic field in the SG rotor. The Automatic Voltage Regulator (AVR) controls the excitation current to adjust the terminal voltage of the SG. Different models exist for this system, as listed in [27]. We consider the Simple Exciter model of the excitation system (exciter and AVR) represented in Fig. 2.3. The input is made by the difference between the reference

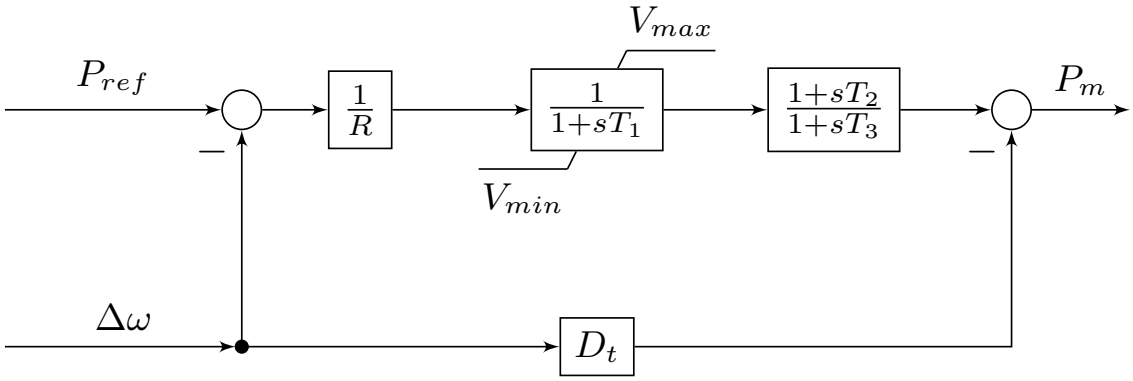

Figure 2.2: IEEE TGOV1 model diagram

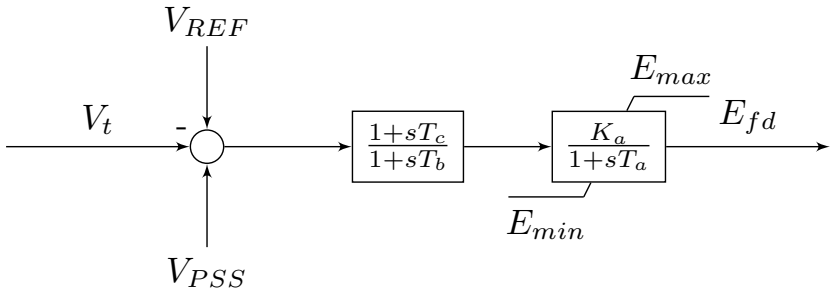

Figure 2.3: Simple Exciter model

voltage V_{ref} and the output voltage V_t plus the power system stabilizer output V_{PSS}. The first block represents the AVR, in which T_c and T_b are its time constants, while the second one the exciter, in which K_a and T_a are respectively the gain and the time constant of the exciter. The output is the exciter output voltage.

2.2 Power System Stabilizers

The Power System Stabilizer (PSS) is the most used approach to control and to damp low-frequency oscillations. They introduce a component torque in the synchronous machine through the excitation circuit that acts as a damping torque.
Different structures exist in the literature and on the market. They differ in the number of inputs, in the signals used as inputs and in the control structure. A list can be found in [27]. We consider the simpler one, called PSS1A and shown in Fig. 2.4, which has only one input, the rotor speed deviation, and it is composed of a wash-out filter and two lead-lag blocks for the phase compensation. The washout filter is needed to filter low-frequency components leaving the steady state output unaltered. Usually, the time constant T_w takes values between 1 and 20 seconds. We set it to 10 seconds for our simulations. The lead-lag blocks are the control part responsible for generating the correct signal to introduce the damping torque and reduce the oscillations.
The parameters of the lead-lag blocks and the gain of the PSS are the fundamental parameters that must be correctly tuned to obtain the desired performance. Various

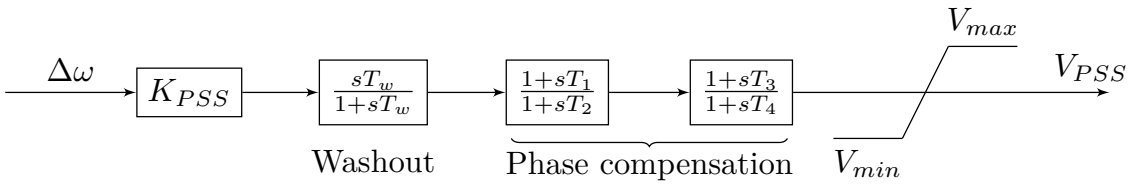

Figure 2.4: PSS1A diagram

approaches for tuning these parameters exist in the literature. The classical methods are the "GEP" method, the "P-Vr" method and the residue method [28]. In the first method, the phase compensation parameters are computed from the transfer function from the voltage reference to the terminal voltage. In the second, they are computed from the transfer function from the voltage reference to the electric power when the shaft dynamics of all machines are disabled. Finally, in the residue method, they are computed by analysing the residue of the transfer function from the voltage reference to the root speed. Since we will identify a model for this input-output relation, we will use the last method to re-tune the parameters of the PSS.

2.3 Modal Analysis

The modal analysis [29] of the power system can be used to understand the oscillatory behaviour of the system, that is mainly related to SGs dynamics.
Suppose we have a complete description of the power system, the equations of the system can be written as in (2.1), where the first set of equations is the set of differential equations and the second one is the set of algebraic equations. They are composed of the equations of the synchronous machines, the control devices, the network, the loads and in general all the devices that contribute to the dynamics of the system. The vector $\mathbf{x}$ is the state vector containing for example the rotor angle and speed variables. The vector $\mathbf{y}$ is the set of algebraic variables and the vector $\mathbf{u}$ contains the system input.

$$\begin{cases} \dot{\mathbf{x}} = \mathbf{f}(\mathbf{x}, \mathbf{y}, \mathbf{u}) \\ \mathbf{0} = \mathbf{g}(\mathbf{x}, \mathbf{y}, \mathbf{u}) \end{cases} \tag{2.1}$$

In general, they are highly non-linear but they can be linearised around the operating point of the system and written as a linear state-space model as shown in (2.2). Then, from the matrix $\mathbf{A}$, we can study the dynamical behavior of the system, including the identification of low-frequency oscillations. In particular, we can analyse the frequency and damping of the oscillations and which machines are involved.

$$\dot{\mathbf{x}} = \mathbf{A}\mathbf{x} + \mathbf{B}\mathbf{u} \tag{2.2}$$

The eigenvalues of the state matrix $\mathbf{A}$ are the scalar values $\lambda_i \in \mathbb{C}$ that solves equation (2.3), for some eigenvector $\mathbf{v}_i$ different from zero.

$$\mathbf{A}\mathbf{v}_i = \lambda_i \mathbf{v}_i \tag{2.3}$$

Each complex eigenvalue of the system is associated with an oscillation mode. Let $\lambda = \sigma + i\omega$ be a complex eigenvalue of the system, then the frequency f and damping coefficient ξ of the associated mode are given in (2.4). The damping coefficient ξ is smaller than one and represents the oscillation decay. If it is close to zero then the oscillation is badly damped and it takes a large time to disappear, instead if it is close to one the oscillation is well damped. Usually, it is also expressed in percentage.

$$f = \frac{\omega}{2\pi}, \quad \xi = \frac{-\sigma}{\sqrt{\sigma^2 + \omega^2}} \tag{2.4}$$

We suppose the matrix $\mathbf{A}$ can be diagonalized as shown in (2.5), where $\mathbf{V}$ is the eigenvector matrix $\mathbf{V} = [\mathbf{v}_1 \ \dots \ \mathbf{v}_n]$ and $\mathbf{\Lambda}$ is a diagonal matrix whose elements are the eigenvalues.

$$\mathbf{V}^{-1}\mathbf{A}\mathbf{V} = \mathbf{\Lambda} \tag{2.5}$$

We can also define the matrix $\mathbf{W} = [\mathbf{w}_1 \ \dots \ \mathbf{w}_n]^T = \mathbf{V}^{-1}$, where the vectors $\mathbf{w}_i$ are the left eigenvectors of $\mathbf{A}$, since they solve $\mathbf{w}_i^T\mathbf{A} = \mathbf{w}_i^T\lambda_i$.
Then, by defining the new state variable $\mathbf{z} = \mathbf{W}\mathbf{x}$, the state equation is as in (2.6). The free evolution of $\mathbf{z}$ is given by $\dot{\mathbf{z}} = \mathbf{\Lambda}\mathbf{z}$, or component wise as $\dot{z}_i = \lambda_i z_i$, where z_i is the i-th component of $\mathbf{z}$, whose solution is $z_i(t) = e^{\lambda_i t} z_i(0)$.

$$\dot{\mathbf{z}} = \mathbf{\Lambda}\mathbf{z} + \mathbf{W}\mathbf{B}\mathbf{u} \tag{2.6}$$

In this way, each variable z_i corresponds to a mode of the system characterized by the eigenvalue λ_i. Therefore, coming back to the original state vector, obtainable from $\mathbf{z}$ as $\mathbf{x} = \mathbf{V}\mathbf{z}$, each component x_k is connected to the mode of the system through equation (2.7). The coefficient v_{ki} of the right eigenvector $\mathbf{v}_k$ gives information about how the i-th mode is present in the k-th state. In particular, the higher the magnitude $|v_{ki}|$ is, the more the i-th mode participates in the k-th state evolution. Moreover the angle $\angle v_{ki}$ gives the "direction" of the variation caused by the excitation of the mode. By plotting the complex components related to the machine rotor speed state of the vector $\mathbf{v}_i$, we can identify the type of oscillation and which machines are oscillating against the others. In particular, if two machines have almost the same angle they are oscillating together, instead if the angles differs by 180 degrees then they are oscillating one against the other. For this reason, the right eigenvectors $\mathbf{v}_i$ are also called mode shapes.

$$x_k(t) = \sum_i v_{ki} z_i(t) \tag{2.7}$$

We are not only interested from which state we can observe one mode, but also in the reverse problem: which state can have an impact on a particular mode. Similar to (2.7), we can write the reverse equation as in (2.8). In this case, the components w_{ik} of the left eigenvector $\mathbf{w}_k$ give the relation between the k-th state and the i-th mode.

$$z_i(t) = \sum_k w_{ik} x_k(t) \tag{2.8}$$

Moreover, by combining the right and left eigenvectors, we can introduce the normalized participation as in (2.9), which measures how much the i-th mode and the k-th state variable are connected, considering both observability and controllability. For the fixed i-th mode, we compare p_{ki} for the different states indexed by k. The higher participation factor identifies the state, and the relative machine, that is more connected to the mode, both considering the observability given by v_{ki} and the controllability given by w_{ki}. This gives indication about where we can act the control a particular mode of the system.

$$p_{ki} = \frac{|v_{ki} w_{ki}|}{\sum_i |v_{ki} w_{ki}|} \tag{2.9}$$

Finally, to understand if a mode is related to a low-frequency power oscillation we compare the participation factor related to the rotor motion of the machine to their total sum by defining the correlation ratio, as in (2.10). In the nominator, we have the sum of the participation factors related to the rotor angle and rotor speed state. If $\eta_i \approx 1$ then we can consider the relative mode as a low-frequency power oscillation mode.

$$\eta_i = \frac{p_{ki}(x_k = \delta) + p_{ki}(x_k = \omega)}{\sum_k p_{ki}} \tag{2.10}$$

To conclude, by performing this analysis, we can understand the oscillatory behaviour of the system. However, it requires a complete description of the power system that is not always available. We apply this analysis to the test case in Chapter 4.

3

System Identification

In this chapter the general system identification problem is presented and two different approaches are considered. The first considers transfer function model structures and we use the prediction error minimization (PEM) method to estimate the model parameters. The second considers state-space model structure and we use different subspace methods for the system identification.

3.1 Introduction

With system identification (SI) we mean the procedure to learn a model from data. A model is a mathematical description of the system, establishing a relation between some observable variables of the system. In general, there are two types of variables that can be measured:

- exogenous variables or input u
- explained variables or output y.

There are three general ingredients in the system identification procedure:

- a model class, or model structure, containing the possible model that can explain the relation between inputs and outputs,
- the data, inputs and outputs, collected in an experiment
- a criterion to choose the best model in the model class that can explain the relation between the inputs and the outputs

In general, in a real system there are some other non observable variables that influence the relation between the input u and the output y, and they can be modeled as external disturbances.

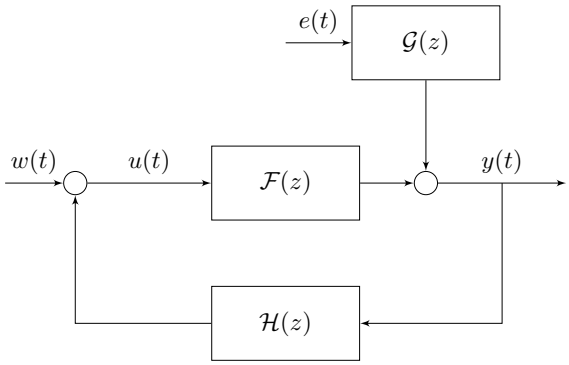

Figure 3.1: Model with feedback

We consider a general linear model with feedback to describe the system which equations are shown in (3.1).

$$\begin{cases} y(t) = \mathcal{F}(z)u(t) + \mathcal{G}(z)e(t) \\ u(t) = \mathcal{H}(z)y(t) + w(t) \end{cases} \tag{3.1}$$

Here $\mathcal{F}(z)$ models the plant to be identified, $\mathcal{G}(z)e(t)$ models disturbances, and $\mathcal{H}(z)$ is the feedback controller. Meanwhile, $w(t)$ is a reference signal to excite the system, and $u(t)$ and $y(t)$ are the input and the output of system, respectively. The diagram of this general model is reported in Fig. 3.1. $\mathcal{F}(z)$, $\mathcal{G}(z)$ and $\mathcal{H}(z)$ are causal transfer functions of the form (3.2), where z^{-1} is the *backward shift operator*.

$$\mathcal{A}(z) = \sum_{k=0}^{\infty} a_k z^{-k}, \quad a_k \in \mathbb{R} \tag{3.2}$$

It means that the multiplication between a transfer function $\mathcal{A}(z)$ and a discrete time signal $x(t)$ is equivalent to (3.3).

$$\mathcal{A}(z)x(t) = \sum_{k=0}^{\infty} a_k z^{-k} x(t) = \sum_{k=0}^{\infty} a_k x(t-k) \tag{3.3}$$

The system identification problem is to estimate the plant model $\mathcal{F}(z)$ and the disturbances model $\mathcal{G}(z)e(t)$ from measurements of the input $u(t)$ and the output $y(t)$, while the controller $\mathcal{H}(z)$ is assumed to be known and necessary to ensure that the plant operates in safe conditions.

For a correct identification the input signal must be rich in term of frequency content to excite all the dynamics of the system. The most used reference signals are gaussian white noise, random binary signal and multi sines signal. A complete description can be found in [30].

Another important step in the identification is the pre-processing of the input-output data before applying the identification algorithms. Usually, it consists of filtering, dec-

imation, and detrending. Filtering can be used to reduce high-frequency components or to remove known dynamics. Decimation consists of the down-sampling of the data to avoid numerical problems. Finally, detrending is used to remove offsets and trends.

After the identification, some techniques can be used to understand if the identified model is good or instead we have to modify the experiment or change the model structure and identification method. A simple validation is to compare the measured output and the one predicted by the identification model. A more advanced technique is the so call residual analysis [30], in which we check some properties of the residuals, the errors between the measured and predicted output. If we have estimated a good model, we expect that the residuals are close to white noise. So, through the auto-correlation test, we check that the auto-correlation function is inside the confidence interval of the corresponding estimates, meaning that the residuals are uncorrelated. Moreover, using the cross-correlation test we check that the residuals are uncorrelated to the past input as one can expect. Also in this test, we check that the cross-correlation function is inside the confidence interval.

3.2 Transfer function model structure and PEM method

In this approach, $\mathcal{F}(z)$ and $\mathcal{G}(z)$ are parameterized as rational transfer functions through the parameter θ. This defines the model structure $\mathcal{M} := \{\mathcal{M}(\theta), \theta \in \Theta\}$, where Θ is the parameter set that can be chosen to impose some constraints, like the stability of the system. Different structures can be used, as described in the following paragraphs.

ARX Model It is a simple input-output relation that can be obtained writing the model as a linear difference equation, as shown in (3.4).

$$\begin{aligned} y(t)+a_1 y(t-1) + \cdots + a_{n_A} y(t-n_A) &= b_0 u(t-n_k) \\ + b_1 u(t-1-n_k) + \cdots + b_{n_B-1} u(t-n_B+1-n_k) &+ e(t) \end{aligned} \tag{3.4}$$

The parameters that define the model are $\theta = [a_1 \dots a_{n_A} b_0 \dots b_{n_B-1}]$, meanwhile n_A and n_B define the orders of the model, and n_k is the input delay. Defining the transfer functions shown in (3.5), the model structure can be written as in (3.6).

$$A(z) = 1 + \sum_{k=1}^{n_A} a_k z^{-k} \qquad B(z) = \sum_{k=0}^{n_B-1} b_k z^{-k}, \tag{3.5}$$

$$\mathcal{M}(\theta) \; : \; A(z)y(t) = B(z)u(t-n_k) + e(t) \tag{3.6}$$

ARMAX Model Further developing the previous model, we could add flexibility to describe the properties of the disturbance term by assuming that the output at

time instant t depends also on the past disturbances. Therefore, the linear difference equation can be written as in (3.7).

$$\begin{aligned} y(t)+a_1 y(t-1)+\cdots+a_{n_A} y(t-n_A) = b_0 u(t-n_k)+b_1 u(t-1-n_k)+\ldots \\ +b_{n_B-1} u(t-n_B+1-n_k)+e(t)+c_1 e(t-1)+\cdots+c_{n_C} e(t-n_C) \end{aligned} \tag{3.7}$$

The parameters that define the model are $\theta = [a_1 \ldots a_{n_A} b_0 \ldots b_{n_B-1} c_1 \ldots c_{n_C}]$, with n_A,n_B and n_C defining the orders of the model, and n_k is the input delay. Defining the transfer functions shown in (3.8), the model structure can be written as in (3.9).

$$A(z) = 1+\sum_{k=1}^{n_A} a_k z^{-k} \qquad B(z) = \sum_{k=0}^{n_B-1} b_k z^{-k} \qquad C(z) = 1+\sum_{k=1}^{n_C} c_k z^{-k} \tag{3.8}$$

$$\mathcal{M}(\theta) \,:\, A(z)y(t) = B(z)u(t-n_k)+C(z)e(t) \tag{3.9}$$

Notice that the ARX model can be seen as a particular case of ARMAX model, with $n_C = 0$.

Output-Error (OE) Model Another option is to assume that the disturbance does not enter in the dynamics between the input and the output, but it consists of measurements disturbance. In this case, defining the transfer functions shown in (3.10), the model structure is shown in (3.11).

$$B(z) = \sum_{k=0}^{n_B-1} b_k z^{-k} \qquad F(z) = 1+\sum_{k=1}^{n_F} f_k z^{-k} \tag{3.10}$$

$$\mathcal{M}(\theta) \,:\, y(t) = \frac{B(z)}{F(z)}u(t-n_k)+e(t) \tag{3.11}$$

The parameters that define the model are $\theta = [f_1 \ldots f_{n_F} b_0 \ldots b_{n_B-1}]$, meanwhile n_F and n_B define the orders of the model, and n_k is the input delay.

Box-Jenkins (BJ) Model The last model is derived from the OE model, assuming a more complex model for the disturbance. Indeed, defining the transfer functions shown in (3.12), the model structure is shown in (3.13).

$$B(z) = \sum_{k=0}^{n_B-1} b_k z^{-k} \quad F(z) = 1+\sum_{k=1}^{n_F} f_k z^{-k} \quad C(z) = 1+\sum_{k=1}^{n_C} c_k z^{-k} \quad D(z) = 1+\sum_{k=1}^{n_D} d_k z^{-k} \tag{3.12}$$

$$\mathcal{M}(\theta) \,:\, y(t) = \frac{B(z)}{F(z)}u(t-n_k)+\frac{C(z)}{D(z)}e(t) \tag{3.13}$$

The parameters that define the model are $\theta = [f_1 \dots f_{n_F} b_0 \dots b_{n_B-1}, c_1 \dots c_{n_C} d_1 \dots d_{n_D}]$, with n_F,n_B, n_C and n_D defining the orders of the model, and n_k is the input delay. The OE model can be seen as a BJ model with $n_C = n_D = 0$.

3.2.1 PEM method

The prediction error minimization (PEM) method is a method to identify the unknown parameters of the system. Considering the general model structure shown in (3.14), where the parametrization of the model can correspond to either BJ, OE, ARMAX or ARX model structure.

$$\mathcal{M}(\theta) \; : \; y(t) = \mathcal{F}_\theta(z)u(t) + \mathcal{G}_\theta(z)e(t), \tag{3.14}$$

At time t we have collected the past data $\{(y(s), u(s)), s < t\}$. Then, it can be shown [31] that the minimum squared error prediction of $y(t)$ given by the past data is (3.15), where $\mathcal{G}_{1,\theta}(z) = \mathcal{G}_\theta(z) - 1$. With minimum squared error prediction we mean the best possible prediction of $y(t)$ from the past data with respect to the expectation of the squared error between the measured and predicted output.

$$\hat{y}_\theta(t|t-1) = \mathcal{G}_\theta(z)^{-1}\mathcal{G}_{1,\theta}(z)y(t) + \mathcal{G}_\theta(z)^{-1}\mathcal{F}_\theta(z)u(t) \tag{3.15}$$

We define the prediction error as $\epsilon_\theta(t) := y(t) - \hat{y}_\theta(t|t-1)$. Assuming to have collected the data $\mathbf{u}^N$ and $\mathbf{y}^N$ (3.16), then the PEM estimate $\hat{\theta}_{PEM}$ is given by (3.17), by solving the optimization problem which minimizes the mean square prediction error $V_N(\theta)$ with respect to the unknown parameters.

$$\mathbf{u}^N = [u(1) \dots u(N)]^T, \quad \mathbf{y}^N = [y(1) \dots y(N)]^T \tag{3.16}$$

$$\hat{\theta}_{PEM}(\mathbf{u}^N, \mathbf{y}^N) = \underset{\theta \in \Theta}{\arg\min}\, V_N(\theta), \quad V_N(\theta) = \frac{1}{N}\sum_{t=1}^{N} \epsilon_\theta(t)^2 \tag{3.17}$$

3.2.2 PEM method for ARX model structure

For the ARX model structure, the solution of the PEM estimate (3.17) can be written in closed form since the minimum squared error predictor (3.15) is linear with respect to the unknown parameters. Indeed, it can be written as in (3.18), where without loss of generality we consider the input delay n_k equal to one.

$$\hat{y}_\theta(t|t-1) = -\sum_{k=1}^{n_A} a_k y(t-k) + \sum_{k=0}^{n_B-1} b_k u(t-k-1) \tag{3.18}$$

Defining the regression vector $\phi(t)$ (3.19), we have that (3.18) can be written as $\hat{y}_\theta(t|t-1) = \phi(t)^T\theta$.

$$\phi(t) := \begin{bmatrix} -y(t-1) & \dots & -y(t-n_A) & u(t-1) & \dots & u(t-n_B) \end{bmatrix}^T \tag{3.19}$$

Assume to have collected the data $\mathbf{u}^N, \mathbf{y}^N$. Then we can define the regression matrix $\mathbf{\Phi}$ and the prediction error vector $\bar{\epsilon}_\theta$ as in (3.20). The cost function $V_N(\theta)$ in (3.17) can be written as (3.21).

$$\mathbf{\Phi} := \begin{bmatrix} \phi(1)^T \\ \vdots \\ \phi(N)^T \end{bmatrix} \quad \bar{\epsilon}_\theta := \begin{bmatrix} \epsilon_\theta(1) \\ \vdots \\ \epsilon_\theta(N) \end{bmatrix} = \mathbf{y}^N - \mathbf{\Phi}\theta. \tag{3.20}$$

$$V_N(\theta) = \frac{1}{N}\sum_{t=1}^{N} \epsilon_\theta(t)^2 = \frac{1}{N}\|\bar{\epsilon}_\theta\|^2 = \frac{1}{N}\|\mathbf{y}^N - \mathbf{\Phi}\theta\|^2 \tag{3.21}$$

Therefore the prediction error estimate can be written as the solution of (3.22), which is the standard least square error problem where the solution is given in (3.23), assuming $\mathbf{\Phi}$ has full column rank.

$$\hat{\theta}_{PEM}(\mathbf{y}^N, \mathbf{u}^N) = \arg\min_{\theta \in \Theta} \|\mathbf{y}^N - \mathbf{\Phi}\theta\|^2 \tag{3.22}$$

$$\hat{\theta}_{PEM}(\mathbf{y}^N, \mathbf{u}^N) = (\mathbf{\Phi}^T\mathbf{\Phi})^{-1}\mathbf{\Phi}^T\mathbf{y}^N \tag{3.23}$$

3.2.3 PEM method for ARMAX, BJ and OE model structure

In this case, the predictor (3.15) is not linear with respect to the parameters, therefore an analytic form of $\hat{\theta}_{PEM}$ is not obtainable. To solve the optimization problem (3.17), different algorithms can be used to compute the solution, as for example gradient descent method or Newton method. The discussion of these algorithms is out of the scope of this thesis, but it can be found in [30].

3.3 Subspace methods for identification of state space models

Subspace identification methods are a class of algorithms to identify the model in state-space based on algebraic properties. Consider the discrete time state-space system, shown in 3.24. Here $\mathbf{x} \in \mathbb{R}^n$ is the state vector, $\mathbf{u} \in \mathbb{R}^m$ is the input, $\mathbf{y} \in \mathbb{R}^l$ is the output, $\mathbf{w} \in \mathbb{R}^n$ and $\mathbf{v} \in \mathbb{R}^l$ are the state and output disturbances, and $\mathbf{A}, \mathbf{B}, \mathbf{C}, \mathbf{D}$ are the state space matrices. The aim is to estimate the state space matrices from the collected

data $\mathbf{u}^N, \mathbf{y}^N$.

$$\begin{cases} \mathbf{x}(t+1) = \mathbf{A}\mathbf{x}(t) + \mathbf{B}\mathbf{u}(t) + \mathbf{w}(t) \\ \mathbf{y}(t) = \mathbf{C}\mathbf{x}(t) + \mathbf{D}\mathbf{u}(t) + \mathbf{v}(t) \end{cases} \tag{3.24}$$

We present two different type of subspace methods, namely the Multivariable Output Error State Space (MOESP) method [32] and the Canonical Variate Analysis (CVA) method [33]. These methods can be unified in the same procedure and the only difference is the choice of some weighting matrices [34]. These subspace algorithms are based on the following steps:

- From the input-output data, the extended observability matrix defined in (3.25) is estimated. The parameter r is the prediction horizon.

$$\mathbf{O}_r = \begin{bmatrix} \mathbf{C} \\ \mathbf{CA} \\ \vdots \\ \mathbf{CA}^{r-1} \end{bmatrix} \tag{3.25}$$

- From the estimated of the observability matrix, namely $\hat{\mathbf{O}}_r$, the matrices $\mathbf{A}$ and $\mathbf{C}$ can be estimated: the estimate $\mathbf{C}$ is the first block row of $\hat{\mathbf{O}}_r$, meanwhile the estimate $\mathbf{A}$ can be computed by solving a least square problem.
- Finally, the estimate of the matrices $\mathbf{B}$ and $\mathbf{D}$ can be computed solving an other least square problem given in equation (3.26), where the output predictor is given in (3.27) that is computed knowing the estimate $\hat{\mathbf{C}}$ and $\hat{\mathbf{A}}$.

$$[\hat{\mathbf{B}}, \hat{\mathbf{D}}] = \arg\min_{\mathbf{B},\mathbf{D}} \frac{1}{N} \sum_{t=1}^{N} ||\mathbf{y}(t) - \hat{\mathbf{y}}(t|t-1)||^2 \tag{3.26}$$

$$\hat{\mathbf{y}}(t|t-1) = \hat{\mathbf{C}}(z\mathbf{I} - \hat{\mathbf{A}})^{-1}\mathbf{B}\mathbf{u}(t) + \mathbf{D}\mathbf{u}(t) \tag{3.27}$$

The most critical part is the estimation of the observability matrix $\mathbf{O}_r$. We present a brief summarize of the procedure of this step, meanwhile the detail of the other two step can be found in [30]. We start by writing the output sequence from time t to $t + r - 1$ as in (3.28), which is derived by iterating the state-space equation (3.24), where the vector $\mathbf{V}(t)$ collects all the factors given by the disturbances.

$$\begin{bmatrix} \mathbf{y}(t) \\ \mathbf{y}(t+1) \\ \vdots \\ \mathbf{y}(t+r-1) \end{bmatrix} = \begin{bmatrix} \mathbf{C} \\ \mathbf{CA} \\ \vdots \\ \mathbf{CA}^{r-1} \end{bmatrix} \mathbf{x}(t) + \begin{bmatrix} \mathbf{D} & 0 & \cdots & 0 \\ \mathbf{CB} & \mathbf{D} & \cdots & 0 \\ \vdots & \ddots & \ddots & \vdots \\ \mathbf{CA}^{r-2}\mathbf{B} & \cdots & \mathbf{CB} & \mathbf{D} \end{bmatrix} \begin{bmatrix} \mathbf{u}(t) \\ \mathbf{u}(t+1) \\ \vdots \\ \mathbf{u}(t+r-1) \end{bmatrix} + \mathbf{V}(t) \tag{3.28}$$

It can written in matrix form as (3.29), where the matrix are defined accordingly.

$$\mathbf{Y}_r(t) = \mathbf{O}_r\mathbf{x}(t) + \mathbf{S}_r\mathbf{U}_r(t) + \mathbf{V}(t) \tag{3.29}$$

This last equation relates the input-output data through the matrices $\mathbf{O}_r$ and $\mathbf{S}_r$ and in particular can be used to get the estimate $\hat{\mathbf{O}}_r$. Assume to have collect the data

$\mathbf{u}^{N+r-1}, \mathbf{y}^{N+r-1}$, then we stack the equations in (3.29) from t equal to zero up to N. The resulting equation is shown in (3.30) where the matrices $\mathbf{Y}$, $\mathbf{U}$, $\mathbf{X}$ and $\mathbf{V}$ are defined in (3.31)-(3.32).

$$\mathbf{Y} = \mathbf{O}_r\mathbf{X} + \mathbf{S}_r\mathbf{U} + \mathbf{V} \tag{3.30}$$

$$\mathbf{Y} = \begin{bmatrix} \mathbf{Y}_r(0) & \cdots & \mathbf{Y}_r(N) \end{bmatrix}, \quad \mathbf{X} = \begin{bmatrix} \mathbf{x}(0) & \cdots & \mathbf{x}(N) \end{bmatrix} \tag{3.31}$$

$$\mathbf{U} = \begin{bmatrix} \mathbf{U}_r(0) & \cdots & \mathbf{U}_r(N) \end{bmatrix}, \quad \mathbf{V} = \begin{bmatrix} \mathbf{V}(0) & \cdots & \mathbf{V}(N) \end{bmatrix} \tag{3.32}$$

From this equation, we would like to isolate the matrix $\mathbf{O}_r$. The first step is to eliminate the second term on the right side of the equation through the projection of the output matrix $\mathbf{Y}$ into the orthogonal complement of the row subspace of $\mathbf{U}$. This is equivalent to multiply equation (3.30) on both side by the projection matrix $\mathbf{\Pi}$ defined in (3.33), which is selected such that $\mathbf{U\Pi} = 0$.

$$\mathbf{\Pi} = \mathbf{I} - \mathbf{U}^T(\mathbf{U}\mathbf{U}^T)^{-1}\mathbf{U} \tag{3.33}$$

The resulting equation is shown in (3.34). Then, the next step is to eliminate the disturbance term $\mathbf{V\Pi}$.

$$\mathbf{Y\Pi} = \mathbf{O}_r\mathbf{X\Pi} + \mathbf{V\Pi} \tag{3.34}$$

We define another matrix $\mathbf{\Phi}$ as in (3.35), where $\phi_s(t)$ is a vector of instrumental variables, and a typical choice is shown in (3.36) where s_1 ans s_2 are the length of the past input and output respectively.

$$\mathbf{\Phi} = \begin{bmatrix} \phi_s(1) & \phi_s(2) & \cdots & \phi_s(N) \end{bmatrix} \tag{3.35}$$

$$\phi_s(t) = \begin{bmatrix} \mathbf{y}(t-1) \\ \vdots \\ \mathbf{y}(t-s_1) \\ \mathbf{u}(t-1) \\ \vdots \\ \mathbf{u}(t-s_2) \end{bmatrix} \tag{3.36}$$

By multiplying equation (3.34) from the right by $\mathbf{\Phi}^T$ and normalizing by N, the matrix $\mathbf{G}$ is defined as (3.37).

$$\mathbf{G} = \frac{1}{N}\mathbf{Y\Pi\Phi}^T = \mathbf{O}_r \underbrace{\frac{1}{N}\mathbf{X\Pi\Phi}^T}_{\mathbf{T}_N} + \underbrace{\frac{1}{N}\mathbf{V\Pi\Phi}^T}_{\mathbf{V}_N} \tag{3.37}$$

It can be shown that, if the data are collected in open-loop, hence the input is uncor-

related with the disturbances, then for $N \to \infty$ the matrix $\mathbf{V}_N$ converges to the zero matrix and $\mathbf{T}_N$ converges to a full rank matrix $\mathbf{T}$. Therefore, considering to have collected enough data such that we can approximate the two matrices with their limits then we can write equation (3.38), in which $\mathbf{G}$ is equal to the product of the observability matrix $\mathbf{O}_r$ and the invertible matrix $\mathbf{T}$ that is just a change of basis in the state representation.

$$\mathbf{G} = \mathbf{O}_r \mathbf{T} \tag{3.38}$$

The matrix $\mathbf{G}$ has dimension $rl \times (ls_1 + ms_2)$ and in general it is larger than the real extended observability matrix that has dimension $rl \times n$, where n is the real order of the system and it is unknown. To reduce the dimension and estimate the order of the system we can resort to the Singular Value Decomposition (SVD). For more flexibility, before applying the SVD we can multiply the matrix $\mathbf{G}$ by two weighting matrices $\mathbf{W_1}$ and $\mathbf{W_2}$. The SVD applied to the matrix after the multiplication is shown in (3.39), where we have already exploited the partition of the matrices based on the selection of the n most significant singular value. The coefficient n will be the order of the identified model.

$$\mathbf{W_1 G W_2} = \begin{bmatrix} \mathbf{P} & \mathbf{P}_\perp \end{bmatrix} \begin{bmatrix} \mathbf{\Sigma}_n & \mathbf{0} \\ \mathbf{0} & \mathbf{\Sigma} \end{bmatrix} \begin{bmatrix} \mathbf{Q} \\ \mathbf{Q}_\perp \end{bmatrix} \tag{3.39}$$

Finally the estimate of the extended observability matrix is given by (3.40), where $\mathbf{R}$ is an arbitrary invertible matrix that will determine the coordinate basis of the state representation.

$$\hat{\mathbf{O}}_r = \mathbf{W}_1^{-1} \mathbf{P R} \tag{3.40}$$

Coming back to the weighting matrices, the post-multiplication by $\mathbf{W_2}$ just corresponds to an other change of basis, meanwhile the pre-multiplication by $\mathbf{W_1}$ is eliminated in (3.40). They have an important role in the space spanned by $\mathbf{P}$, and hence on the quality of the estimates of the system matrices [30]. The MOESP method uses the weighting matrices expressed in (3.41), meanwhile the CVA method uses (3.42).

$$\text{MOESP}: \quad \mathbf{W}_1 = \mathbf{I}, \quad \mathbf{W}_2 = \left(\frac{1}{N} \mathbf{\Phi \Pi \Phi}^T \right)^{-1} \mathbf{\Phi \Pi} \tag{3.41}$$

$$\text{CVA}: \quad \mathbf{W}_1 = \left(\frac{1}{N} \mathbf{Y \Pi Y} \right)^{-1/2}, \quad \mathbf{W}_2 = \left(\frac{1}{N} \mathbf{\Phi \Pi \Phi}^T \right)^{-1/2} \tag{3.42}$$

From the extended observability matrix we can get the state-space matrices by solving two least square problem as said before.

We use this algorithm in the next chapter to identify a low-order model of the power system. We use the Matlab implementation in the System Identification Toolbox [35] where the Akaine Information Criterion (AIC) is used to find the best value for r, s_1 and s_2. Meanwhile, the order n is selected manually from the SVD. To summarize, the

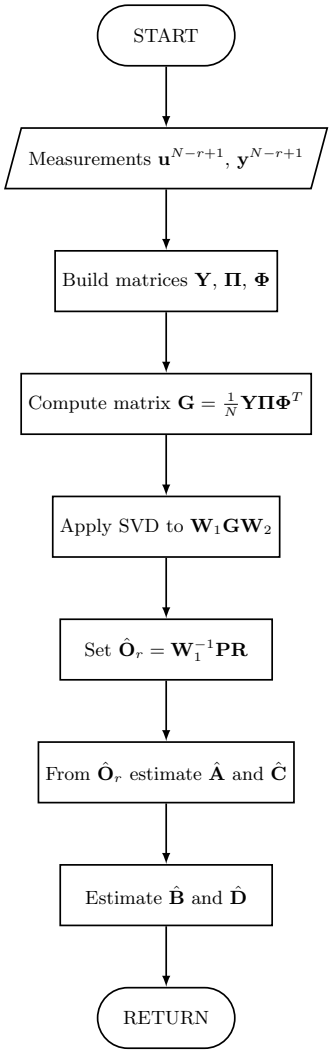

Figure 3.2: MOESP and CVA method flowchart

flowchart of the algorithms is shown in Fig. 3.2.

3.3.1 Predictor-Based Subspace Identification (PBSID) method

In the previous methods we have assumed that the disturbance and the input are independent, but this is not true for closed loop systems. This implies that our estimator will be biased [36]. To overcome this problem different approaches have been developed in the literature. Here we present one of them, the so called Predictive-Based Subspace IDentification (PBSID) method [37],[38]. We use the version based on VARX estimations as illustrated in [39], from where the Matlab implementation has also been taken. It uses a different procedure with respect to the subspace methods presented above and it consist in two steps:

- First, it estimates the state sequence $\mathbf{x}(t)$.
- Secondly, given the state estimate at instant t and $t+1$, it computes the state space matrices $\mathbf{A}$, $\mathbf{B}$, $\mathbf{C}$, $\mathbf{D}$ solving a least square problem.

We consider the equivalent *Kalman predictor form* of the state space system (3.24) written as in (3.43), with $\tilde{\mathbf{A}} = \mathbf{A} - \mathbf{KC}$ and $\tilde{\mathbf{B}} = \mathbf{B} - \mathbf{KD}$.

$$\begin{cases} \mathbf{x}(t+1) = \tilde{\mathbf{A}}\mathbf{x}(t) + \tilde{\mathbf{B}}\mathbf{u}(t) + \mathbf{K}\mathbf{y}(t) \\ \mathbf{y}(t) = \mathbf{C}\mathbf{x}(t) + \mathbf{D}\mathbf{u}(t) + \mathbf{e}(t) \end{cases} \tag{3.43}$$

The matrix $\mathbf{K}$ is the Kalman gain and the random vector $\mathbf{e}(t)$ models the disturbances that are assumed to be white noise. Let us introduce the stacked vector $\mathbf{Z}_p(t)$ defined in (3.44), constructed by the input and output data from the time instant t to $t + p - 1$, where p is the past time window.

$$\mathbf{Z}_p(t) = \begin{bmatrix} \mathbf{z}(t) \\ \mathbf{z}(t+1) \\ \vdots \\ \mathbf{z}(t+p-1) \end{bmatrix}, \quad \mathbf{z}(t) = \begin{bmatrix} \mathbf{u}(t) \\ \mathbf{y}(t) \end{bmatrix} \tag{3.44}$$

Moreover, we can collect the vector just defined, introducing the matrix $\mathbf{Z}$ as in (3.45), where N is the number of samples.

$$\mathbf{Z} = \begin{bmatrix} \mathbf{Z}_p(1) & \dots & \mathbf{Z}_p(N-p) \end{bmatrix} \tag{3.45}$$

Finally, we define the extended controllability matrix and the extended observability matrix in (3.46) and (3.47), where $f \leq p$ is the future time window.

$$\mathcal{K}_p = \begin{bmatrix} \tilde{\mathbf{A}}^{p-1}\bar{\mathbf{B}} & \tilde{\mathbf{A}}^{p-2}\bar{\mathbf{B}} & \dots & \bar{\mathbf{B}} \end{bmatrix}, \quad \bar{\mathbf{B}} = \begin{bmatrix} \mathbf{B} & \mathbf{K} \end{bmatrix} \tag{3.46}$$

$$\mathbf{O}_f = \begin{bmatrix} \mathbf{C} \\ \mathbf{C}\tilde{\mathbf{A}} \\ \vdots \\ \mathbf{C}\tilde{\mathbf{A}}^{f-1} \end{bmatrix} \tag{3.47}$$

The first step of the algorithm is to reconstruct the state sequence. The main assumption used in the PBSID method is to assume $\tilde{\mathbf{A}}^j \approx \mathbf{0}$ for all $j \geq p$. In [40] it is shown that if the system is uniformly exponential stable, the approximation error can be made arbitrary small by choosing p large. With this assumption, the state at instant $t + p$ can be simplified as shown in (3.48).

$$\mathbf{x}(t+p) = \tilde{\mathbf{A}}^p\mathbf{x}(t) + \mathcal{K}_p\mathbf{Z}_p(t) \approx \mathcal{K}_p\mathbf{Z}_p(t) \tag{3.48}$$

Multiplying both side by the observability matrix $\mathbf{O}_f$, we obtain the equation (3.49) that

can be later used to compute the state sequence, provided $\mathbf{O}_f\mathcal{K}_p$ is known.

$$\mathbf{O}_f\mathbf{x}(t+p) = \mathbf{O}_f\mathcal{K}_p\mathbf{Z}_p(t) \tag{3.49}$$

We expand the product $\mathbf{O}_f\mathcal{K}_p$ as in (3.50), where we consider the fact that $\tilde{\mathbf{A}}^j \approx \mathbf{0}$ for j greater or equal to p.

$$\mathbf{O}_f\mathcal{K}_p = \begin{bmatrix} \mathbf{C}\tilde{\mathbf{A}}^{p-1}\bar{\mathbf{B}} & \mathbf{C}\tilde{\mathbf{A}}^{p-2}\bar{\mathbf{B}} & \dots & \dots & \dots & \mathbf{C}\bar{\mathbf{B}} \\ \mathbf{0} & \mathbf{C}\tilde{\mathbf{A}}^{p-1}\bar{\mathbf{B}} & \dots & \dots & \dots & \mathbf{C}\tilde{\mathbf{A}}\bar{\mathbf{B}} \\ \vdots & \ddots & \ddots & \ddots & \ddots & \vdots \\ \mathbf{0} & \dots & \mathbf{0} & \mathbf{C}\tilde{\mathbf{A}}^{p-1}\bar{\mathbf{B}} & \dots & \mathbf{C}\tilde{\mathbf{A}}^{f-1}\bar{\mathbf{B}} \end{bmatrix} \tag{3.50}$$

Notice that the matrix can be obtained only from the elements of the first block row, which is exactly equal to $\mathbf{C}\mathcal{K}_p$, that will be estimated from the input-output data. By taking the approximation (3.48) into the output equation in (3.43), the output can be approximate as in (3.51), or in vector form as in (3.52) by stacking the measurements.

$$\mathbf{y}(t+p) \approx \mathbf{C}\mathcal{K}_p\mathbf{Z}_p(t) + \mathbf{D}\mathbf{u}(t+p) + \mathbf{e}(t+p) \tag{3.51}$$

$$\mathbf{Y} = \mathbf{C}\mathcal{K}_p\mathbf{Z} + \mathbf{D}\mathbf{U} + \mathbf{E}, \quad \mathbf{Y} = \begin{bmatrix} \mathbf{y}(p) \\ \mathbf{y}(p+1) \\ \vdots \\ \mathbf{y}(N) \end{bmatrix}, \mathbf{U} = \begin{bmatrix} \mathbf{u}(p) \\ \mathbf{u}(p+1) \\ \vdots \\ \mathbf{u}(N) \end{bmatrix}, \mathbf{E} = \begin{bmatrix} \mathbf{e}(p) \\ \mathbf{e}(p+1) \\ \vdots \\ \mathbf{e}(N) \end{bmatrix}. \tag{3.52}$$

Therefore, the matrix $\mathbf{C}\mathcal{K}_p$, together with $\mathbf{D}$, can be estimated by solving the linear regression problem (3.53).

$$(\widehat{\mathbf{C}\mathcal{K}_p}, \widehat{\mathbf{D}}) = \underset{\mathbf{C}\mathcal{K}_p,\mathbf{D}}{\arg\min} ||\mathbf{Y} - \mathbf{C}\mathcal{K}_p\mathbf{Z} - \mathbf{D}\mathbf{U}||_F^2 \tag{3.53}$$

Now, given the previous estimate, we can build the estimate $\widehat{\mathbf{O}_f\mathcal{K}_p}$ of the matrix (3.50). Successively, we can compute the state sequence $\widehat{\mathbf{X}}$ from (3.49) by solving the low-rank approximation problem in (3.54), where $\widehat{\mathbf{O}}_f$ is an estimate of the observability matrix.

$$\min ||(\widehat{\mathbf{O}\mathcal{K}_p})\mathbf{Z} - \widehat{\mathbf{O}}_f\widehat{\mathbf{X}}||_F \tag{3.54}$$

To solve this problem, we can resort to the Singular Value Decomposition(SVD), shown in (3.55), to compute the low-rank approximation $\widehat{\mathbf{O}}_f\widehat{\mathbf{X}}$.

$$(\widehat{\mathbf{C}\mathcal{K}_p})\mathbf{Z} = \begin{bmatrix} \mathbf{P} & \mathbf{P}_\perp \end{bmatrix} \begin{bmatrix} \mathbf{\Sigma}_n & \mathbf{0} \\ \mathbf{0} & \mathbf{\Sigma} \end{bmatrix} \begin{bmatrix} \mathbf{Q} \\ \mathbf{Q}_\perp \end{bmatrix} \tag{3.55}$$

The matrix $\mathbf{\Sigma}_n$ contains the n largest singular values from which we can set the order of the estimated model. The orthogonal matrix $\mathbf{Q}$ contains the corresponding row space. By setting the remaining singular values to zero, the observability matrix and the state-sequence can be estimated as in (3.56).

$$\widehat{\mathbf{O}}_f = \mathbf{P}\mathbf{\Sigma}_n^{1/2} \qquad \widehat{\mathbf{X}} = \mathbf{\Sigma}_n^{1/2}\mathbf{Q} \tag{3.56}$$

Finally, we can compute the matrices of the state-space system (3.24), solving the least square problem (3.57) and (3.58), where $\mathbf{E} = \mathbf{Y} - \widehat{\mathbf{C}}\widehat{\mathbf{X}} - \widehat{\mathbf{D}}\mathbf{U}$, meanwhile the matrix $\widehat{\mathbf{D}}$ has been computed in (3.53).

$$\widehat{\mathbf{C}} = \arg\min_{\mathbf{C}} ||\mathbf{Y} - \mathbf{C}\widehat{\mathbf{X}} - \widehat{\mathbf{D}}\mathbf{U}||_F^2 \tag{3.57}$$

$$(\widehat{\mathbf{A}}, \widehat{\mathbf{B}}, \widehat{\mathbf{K}}) = \arg\min_{\mathbf{A},\mathbf{B},\mathbf{K}} ||\mathbf{Y} - \mathbf{A}\widehat{\mathbf{X}} - \widehat{\mathbf{B}}\mathbf{U} - \mathbf{K}\mathbf{E}||_F^2 \tag{3.58}$$

Optimized Algorithm: PBSIDopt

In the optimized version of the PBSID algorithm, the elements that build the matrix (3.50) are obtained from the estimation of a Vector AutoRegressive with eXogenous inputs (VARX) model. The state-space model (3.43) can be re-written as a transfer function model, as shown in (3.59), where the transfer functions are defined in (3.60). The Markov parameters $\mathbf{\Psi}$, described in (3.61), are exactly the elements of (3.50).

$$\begin{aligned} \mathbf{y}(k) &= \mathbf{G}(z)\mathbf{u}(k) + (\mathbf{I} - \mathbf{H}(z))\mathbf{y}(k) + \mathbf{e}(k) \\ \mathbf{G}(z) &= \mathbf{D} + \mathbf{C}(z\mathbf{I} - \tilde{\mathbf{A}})^{-1}\tilde{\mathbf{B}} \\ \mathbf{H}(z) &= \mathbf{I} - \mathbf{C}(z\mathbf{I} - \tilde{\mathbf{A}})^{-1}\mathbf{K} \end{aligned} \tag{3.59}$$

$$\begin{aligned} \mathbf{G}(z, \mathbf{\Psi}) &= \Psi_0^u + z^{-1}\Psi_1^u + z^{-2}\Psi_2^u + \dots \\ \mathbf{H}(z, \mathbf{\Psi}) &= \mathbf{I} - z^{-1}\Psi_1^y - z^{-2}\Psi_2^y - \dots \end{aligned} \tag{3.60}$$

$$\Psi_i^u = \begin{cases} \mathbf{D} & \text{for} \quad i = 0 \\ \mathbf{C}\tilde{\mathbf{A}}^{i-1}\tilde{\mathbf{B}} & \text{for} \quad i > 0 \end{cases} \qquad \Psi_i^y = \mathbf{C}\tilde{\mathbf{A}}^{i-1}\mathbf{K} \tag{3.61}$$

The series in (3.60) can be truncated to a finite number of elements corresponding to the past window p. The approximated one-step ahead predictor is given by equation (3.62) or can be re-written as (3.63).

$$\hat{y}(t|t-1) = \mathbf{G}_p(z, \mathbf{\Psi})u(t) + (\mathbf{I} - \mathbf{H}_p(z, \mathbf{\Psi})y(t) \tag{3.62}$$

$$\hat{y}(t|t-1) = \begin{bmatrix} \Psi_p^u & \Psi_p^y & \dots & \Psi_1^u & \Psi_1^y & \Psi_0^u \end{bmatrix} \begin{bmatrix} \mathbf{z}(t-p) \\ \vdots \\ \mathbf{z}(t-1) \\ \mathbf{u}(t) \end{bmatrix} := \mathbf{\Psi\Phi} \tag{3.63}$$

The unknown Markov parameters $\mathbf{\Psi}$ can be estimated by minimizing the prediction error. That is equivalent to solve the least square problem in (3.64).

$$\min_{\mathbf{\Psi}} ||\mathbf{Y} - \mathbf{\Psi\Phi}||_F^2 \tag{3.64}$$

From the estimated parameters we can build the matrix (3.50) and have the estimate of the matrix $\mathbf{D}$ that is equal to Ψ_0^u. The rest of the algorithm is the same as the standard version of PBSID.
To summarize, the flowchart of both algorithms is shown in Fig. 3.3. This optimized version of the PBSID method has lower computational complexity and it is recommended in case of large MIMO system.

These methods do not use any assumption on the independence between input and disturbance, hence they can be used effectively also for the identification of closed-loop systems. In the next chapter, when we refer to the PBSID method we are considering its optimized version PBSIDopt.

Finally, the PEM method can also applied to state-space models to optimize the estimation and reduce the possible bias. After having choose a parametrization of the state matrices, a problem similar to (3.17) can be built. As for ARMAX, OE and BJ models, the problem is not linear and not convex and iterative algorithms are used to solve the problem. Moreover, since the number of parameters is huge, a good initialization is fundamental to get a proper identification. Usually, a subspace method is used for the initialization, but it has to give already a good estimation so that the PEM method can converge to the right solution and to reduce the computation time.

These algorithms will be used and their performance compared for the identification of a low-order model of the power system, suitable for PSS tuning. Moreover, MOESP method can be adapt to handle only output data, without any input, and it will be used in the validation to identify the power oscillations frequencies and damping factor from ambient data [14].

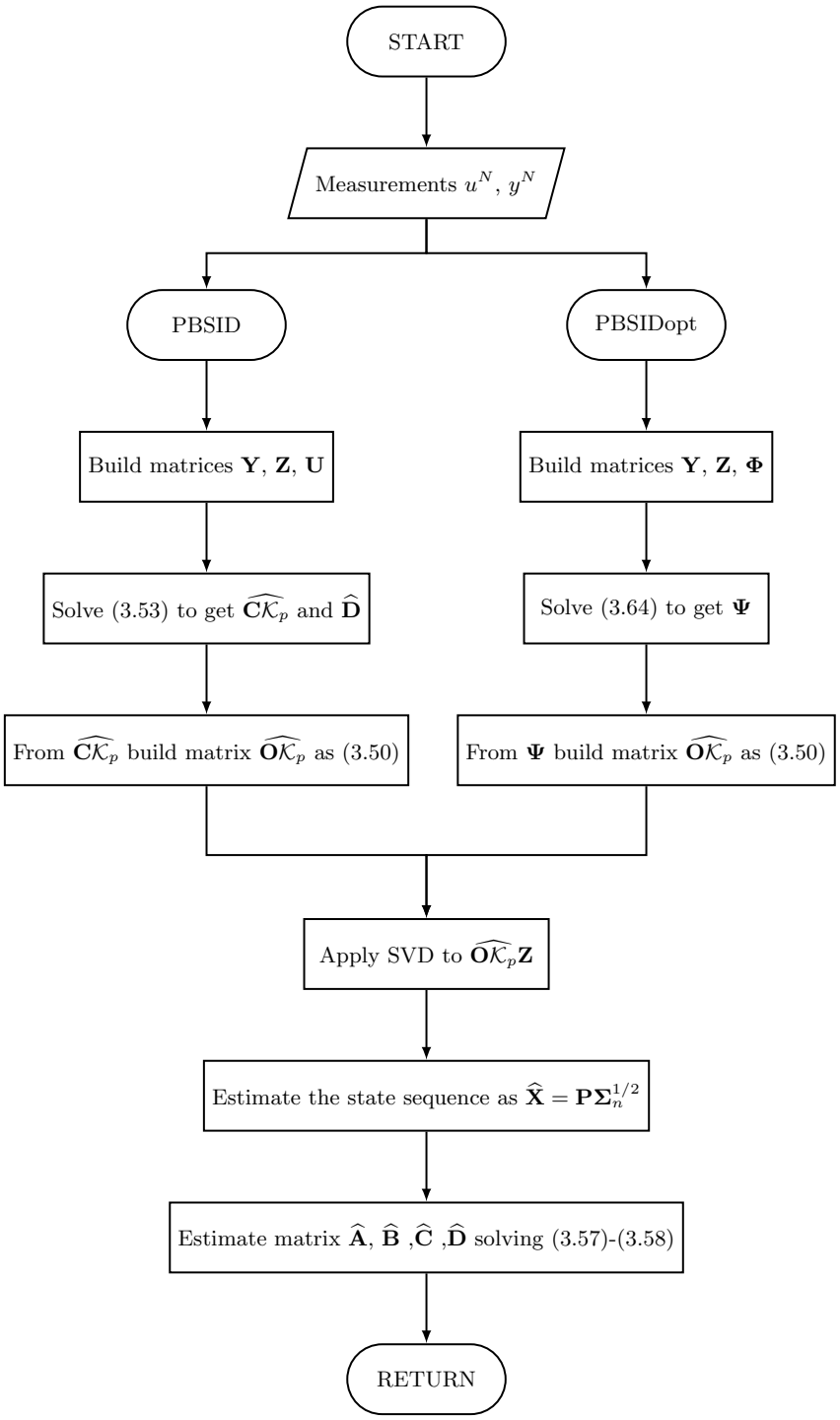

Figure 3.3: PBSID method flowchart

4

Power System Identification for PSS tuning

In this chapter, we introduce the problem of identifing a low-order linear model of the power system, which will be later used in Chapter 5 for the online tuning of the PSSs. We compare the different system identification methods presented in the previous chapter. We consider a modified version of the Two-Area Four-Generators system [41] as test case.

4.1 Introduction

In general, a complete model of the power system is not always available and it can change over time. For example, some lines can be added, the generation can be re-dispatched and also renewable sources can generate power differently based on the weather conditions. Therefore, the Power System Stabilizers may need to be re-tuned based on the actual condition of the system in order to guarantee the required performance. Taking into account that a system model is typically not available, the system identification techniques presented in the previous chapter can be used to identify a low-order model of the power system that can be used to compute the new parameters of the PSSs.
To estimate a model, we need to perturb the system to excite the dynamics. In Fig. 3.1, it corresponds to excite the system with the reference signal $w(t)$ and collect the data sequences $u(t), y(t)$. The excitation signal, also called the probing signal, has to be designed to excite the system only in the frequency range of interest but at the same time to avoid large perturbation that in general are undesired. In our case the range of low-frequency oscillations is the frequency range we are interested in.

Moreover, the identification of systems in close-loop is difficult for mainly two reason. The first is that the feedback modifies the excitation signal making it less

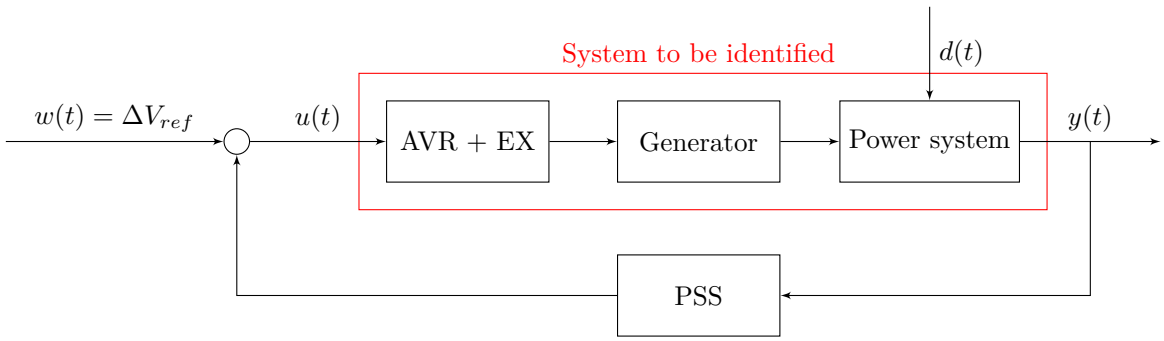

Figure 4.1: Block diagram of the system. Highlighter in red the open loop system to identify

rich of frequency component. The second it makes the input of the open-loop system correlated with the disturbances. So, we test different methods, described in chapter 3, to identify a suitable method that can deal with closed-loop identification and can give a suitable model of the power system.

Let us consider the system diagram in Fig. 4.1. The system to be identified consists in the Automatic Voltage Regulator (AVR), the exciter circuit (EX), the synchronous generator where the PSS is installed and the remaining power system, composed by the all the other devices: other synchronous generators, loads, FACTS, cable, etc.
The reference signal is the voltage reference of the AVR, where the PSS output is added, resulting in the input signal $u(t)$. The input of the PSS is the speed deviation of the synchronous generator. The disturbance signal $d(t)$, which enter in the power system dynamics, models all the variations that happen in the power system around the steady state configuration. By exciting the system through $w(t)$ and collecting the input-output data $u(t)$, $y(t)$, we can identify, using the methods described in the previous chapter, a low-order linear model of the system. We are not interested in the identification of the complete model of the power system (that will be very difficult, if not impossible), but just in a low-order model that can model the relation between the selected input and output and can be used to tune the PSSs. The identification is carried out in discrete time and then the model is transformed in continuous time through the bilinear transformation.

4.2 Two-Area Four-Generator system

To validate and compare the identification methods, we consider a modified version of the Two-Area Four-Generator power system [41], shown in Fig. 4.2. It is composed of four generators, divided in two areas. Each generator is connected to the grid by means of a transformer, which is modelled as an R-L impedance. There are two loads in the system, one connected at bus 7 and the other at bus 9. The generators are modelled with the complete model and they are equipped with the Simple Exciter and the IEEE TGOV1 turbine/governor model, described in Section 2.1. Moreover, in generator 1

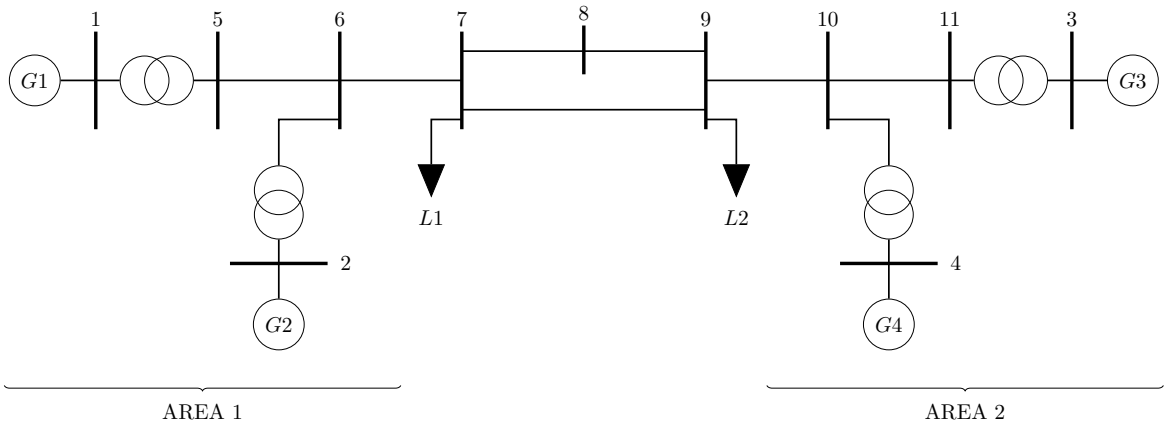

Figure 4.2: Two-Area Four-Generator power system

(G1) a PSS is installed to damp the low-frequency oscillations.

4.2.1 Small Signals Analysis

Before going into the details of the system identification, the small signals analysis is performed to understand the characteristic of this system. Given the parameters of the system and the operation point, the linear system can be obtained in the form (4.1), where $\mathbf{x}$ is the state vector made of 10 state variables for each generator for a total of 40 state variables. The input u is the input made by the sum of the AVR voltage reference and the PSS output at generator 1. The output y is the rotor speed deviation of the same generator, and d is the load variation.

$$\begin{cases} \dot{\mathbf{x}}(t) = \mathbf{A}\mathbf{x}(t) + \mathbf{B}u(t) + \mathbf{B}_d d(t) \\ y(t) = \mathbf{C}\mathbf{x}(t) + \mathbf{D}u(t) + \mathbf{D}_d d(t) \end{cases} \tag{4.1}$$

Having a complete description of the power system, the linear state-space can be obtained analytically as explained in [25]. We use the Power System Toolbox [42] to perform this task and to obtain the state matrices of the power system. With the linear model, we can compute the eigenvalues of $\mathbf{A}$ and perform the modal analysis as described in Section 2.3.

The electromechanical modes are summarized in Table 4.1 and are plotted in Fig. 4.3 . We can notice that the system has a badly damped mode at frequency 0.63 Hz, which is the inter-area mode between the two areas. Moreover, the system has two intra-area modes, one in area 1 and one in area 2, at frequency 1.08 Hz and 1.13 Hz respectively. The participation factors of these modes are computed together with the mode shapes. For each of the three electromechanical oscillation modes, Fig. 4.4 shows the participation factor, meanwhile, Fig. 4.5 shows the mode shape.

As already mentioned, we can see that there is an inter-area mode that includes all the generators where generators 1 and 2 oscillate against generators 3 and 4. Moreover,

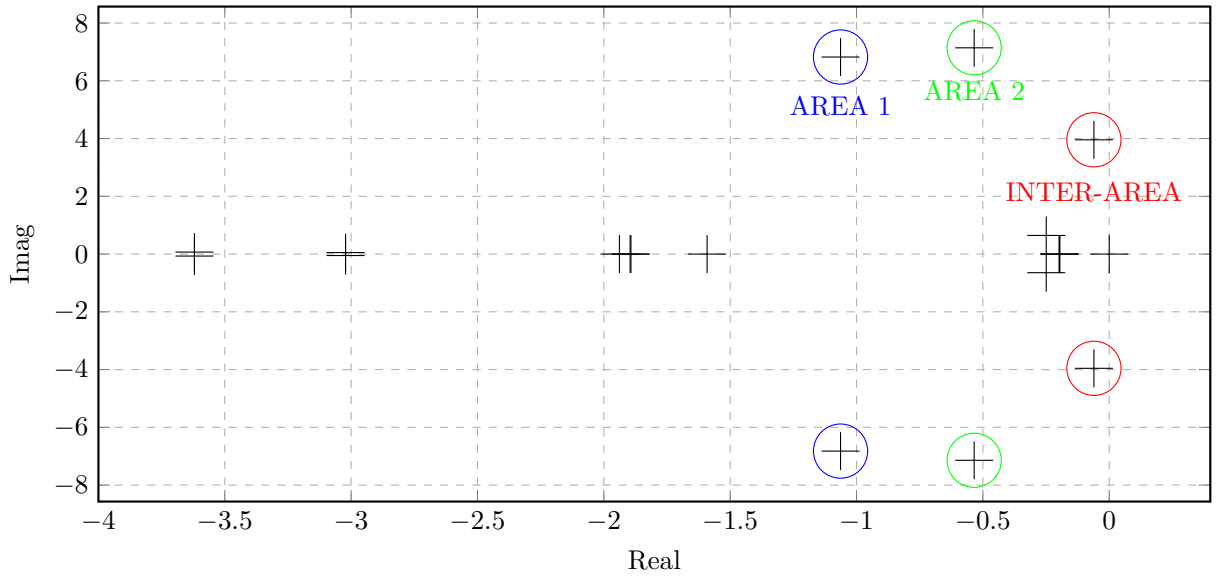

Figure 4.3: Eigenvalues of the Two-Area Four-Generators linearized system

Type	Eigenvalue	Frequency	Damping	Correlation factor	Gen. involved
Inter-area	$-0.062 \pm 3.954i$	0.63 Hz	1.55 %	1	G1-2 vs G3-4
Intra-area	$-1.054 \pm 6.806i$	1.08 Hz	15.31 %	0.9498	G1 vs G2
Intra-area	$-0.545 \pm 7.125i$	1.13 Hz	7.63 %	0.9053	G3 vs G4

Table 4.1: Electromechanical modes of the Two-Area Four-Generators system

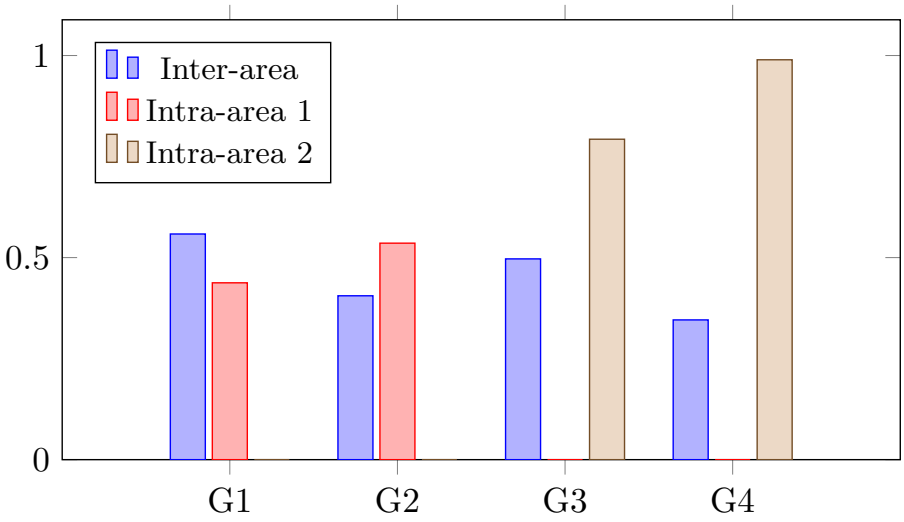

Figure 4.4: Participation factors of the electromechanical modes in the Two-Area Four-Generators system

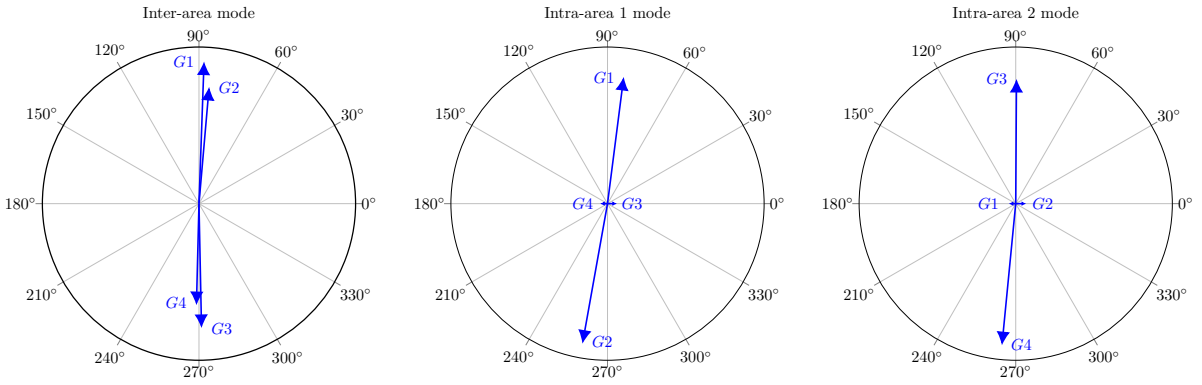

Figure 4.5: Mode shape of the electromechanical modes in the Two-Area Four-Generators system

there is an intra-area mode between generators 1 and 2, and another one between generators 3 and 4. From these plots, we also deduce that the PSS installed at generator 1 can influence the inter-area mode and the intra-area mode of area 1, but not the one of area 2. Moreover, we expect to not be able to identify the oscillation mode in area 2 from local measurements in area 1.

4.2.2 System Identification

A first test is carried out to understand the feasibility of the identification methods and compare them. We excite the system at the reference voltage of the AVR of generator 1, and collect this signal together with the PSS output. We sum them to obtain the input signal $u(t)$.

As excitation signal we choose a multi-sine signal, as in (4.2)-(4.3), with frequencies in the $[0.1, 2]$ Hz range. This excites the system in the frequency range where the low-frequency oscillations are expected. The phases ϕ_k are chosen as (4.3) to minimize the crest factor [30] and to avoid large perturbations. The amplitude of the sines is chosen to avoid rotor speed deviations greater than 10 mHz.

$$w(t) = \sum_{k=0}^{20} 0.0025 \sin(\omega_k t + \phi_k) \tag{4.2}$$

$$\omega_k = 0.1 + \frac{1.9}{20}k, \quad \phi_k = -\frac{k(k+1)}{21}\pi \tag{4.3}$$

The length of the signals, and of the experiment, is 120s. This time window gives satisfactory results but further analysis can be carried out to understand if it can be decreased.

We select as output $\Delta\omega_1$, the speed deviation of generator 1. To the measured output gaussian white noise with a standard deviation of 10^{-5} Hz is added.

The disturbance signals consist in a random load modulation of the two loads with a standard deviation of 10 MW filtered with a 2 Hz low-pass filter. The simulation of

the complete non-linear system is performed using the Power System Toolbox (PST) [35] in Matlab. The data are down-sampled at 10 samples per second, after filtering them through an anti-aliasing filter. Finally, they are scaled so that the returned signals have unitary variance. The input and output data are shown in Fig. 4.6 and 4.7.

The system identification methods, or model structures, considered are the following:

- ARMAX
- BOX-JENKING (BJ)
- PBSID
- MOESP
- CVA

We do not consider ARX and OE model structure because the disturbance model is too simple to describe the disturbances that appear in a power system. For each method, a model of the power system is identified using the input-output data presented above. The order of the model is chosen based on the SVD for subspace methods, while for transfer function models a trial-and-error procedure has been applied until the result was satisfactory. The orders of the models are reported in Table 4.2. To evaluate the performance of the identified models we consider several metrics.

First of all, how well the predicted response of the identified model matches the measured data. Moreover, we consider the normalize root mean square error computed as in (4.4), where y is the output of the system and $\hat{y}$ is the one-step ahead predictor given by the identified model.

$$ERR_y = \frac{||y - \hat{y}||}{||y - \text{mean}(y)||} \tag{4.4}$$

Secondly, the ability of the methods to identify the dominant eigenvalues of the system. We evaluate the normalized euclidean distance on the complex plane (4.5), between the identified eigenvalues $\hat{\lambda}_i$ and the ones of the linearized system λ_i. The set I is the set of low-frequency oscillation modes that we are interested in estimating, i.e. the inter-area and intra-area 1 eigenvalues.

$$ERR_{EIG} = \sum_{i \in I} \frac{||\lambda_i - \hat{\lambda}_i||}{||\lambda_i||} \tag{4.5}$$

Thirdly, the comparison between the frequency response of the identified model and the linearize one. To have a index of this performance, we consider the normalized root mean square error between the frequency responses of the linearized system $H(j\omega)$ and the one of the estimated model $\widehat{H}(j\omega)$, defined in equation (4.6).

$$ERR_\omega = \sum_{\omega=\omega_1}^{\omega_2} \frac{||H(j\omega) - \widehat{H}(j\omega)||}{||H(j\omega)||}, \quad \omega_1 = 0.1\,\text{Hz},\ \omega_2 = 2\,\text{Hz} \tag{4.6}$$

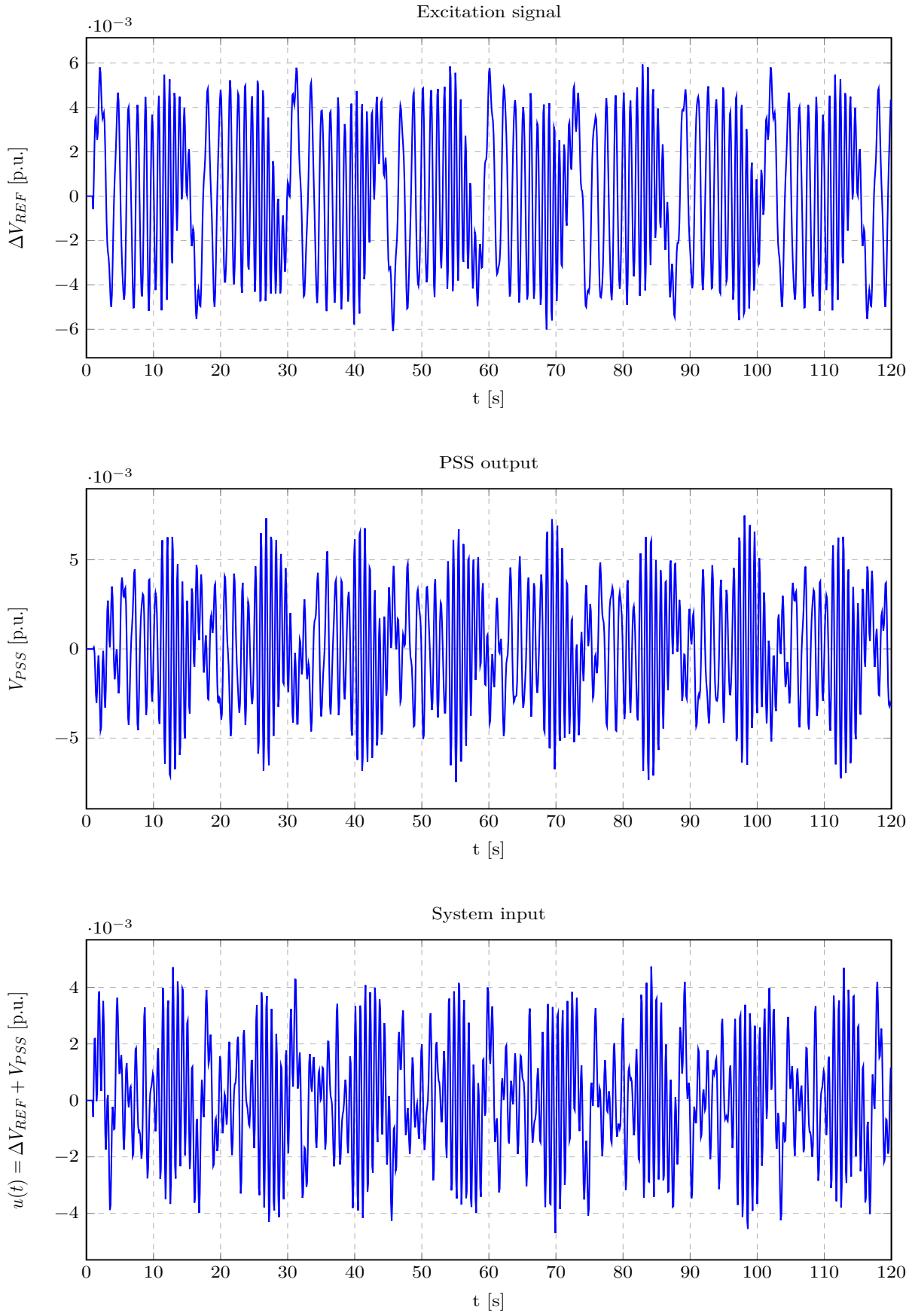

Figure 4.6: Inputs of the system before filtering and down-sampling

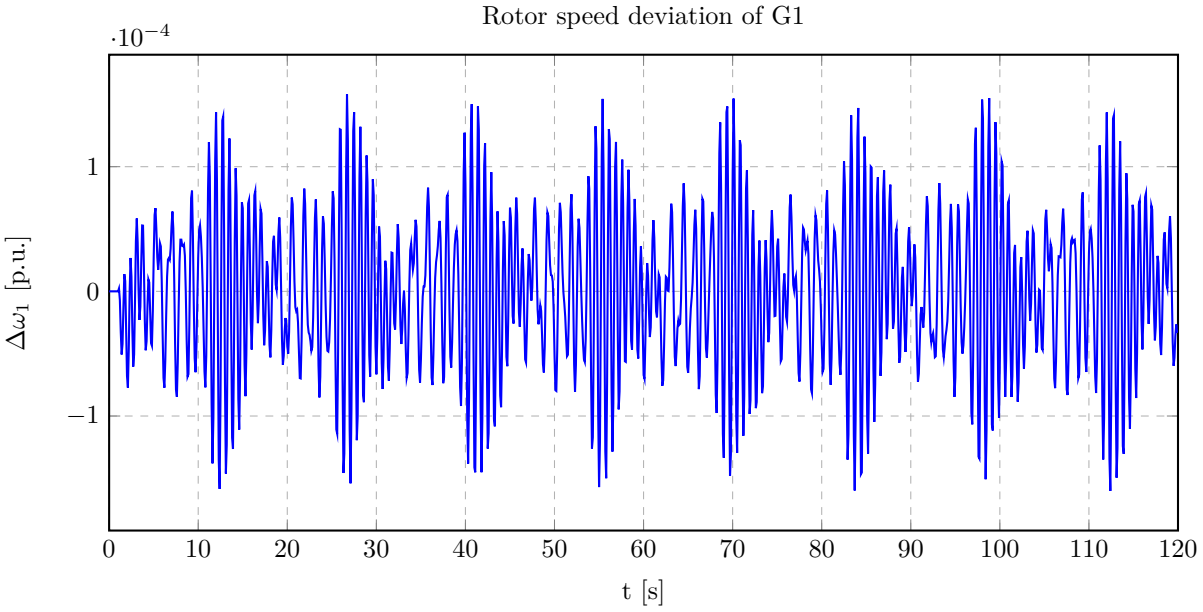

Figure 4.7: Output of the system before filtering and down-sampling

Finally, we perform the auto-correlation and cross-correlation tests briefly described in Section 3.1.

The comparison of the predicted response is shown in Fig. 4.8 compared to the measured output. Meanwhile, in Table 4.2 the error (4.4). All the methods can predict well the output response and have comparable error. In Fig. 4.10 and Fig. 4.11 the eigenvalues are compared and in Table 4.2 the error (4.5) is shown. The MOESP and CVA method are the ones with the worst performance, and PBSID seems to be the more accurate. Moreover, we can notice that not all the eigenvalues are identified but this will not compromise a good design of the PSS based on the identified model. Finally, in Fig. 4.9, the identified frequency response in shown and compared to the one of the linearize system and the error (4.6) is reported in Table 4.2. Also in this case, PBSID has better estimation of the real system, but also ARMAX and BJ performs well. From the eigenvalues and the frequency response, ARMAX and BJ are almost equivalent but the ARMAX is to prefer since it has a simpler model structure. Also MOESP and CVA methods are almost equivalent but CVA gives slightly better results.

For ARMAX and PBSID we perform the residue test, shown in Fig. 4.12. For PBSID both the auto-correlation and the cross-correlation are inside the confidence intervals. Instead the ARMAX model fail the auto-correlation test. This means that this type of model structure can not estimate a good model of the noise and suggests to reject this type of model, as they might have larger sensitivity to noise.

However, to have a better understanding of the statistical properties of the methods, we collect the data from fifty different simulations obtained from different disturbance and noise realizations. We considered the PBSID, ARMAX, CVA methods, that have shown the best performance for each method class, and also we considered the PEM method applied to the estimated model from the PBSID method. In Fig. 4.15 we

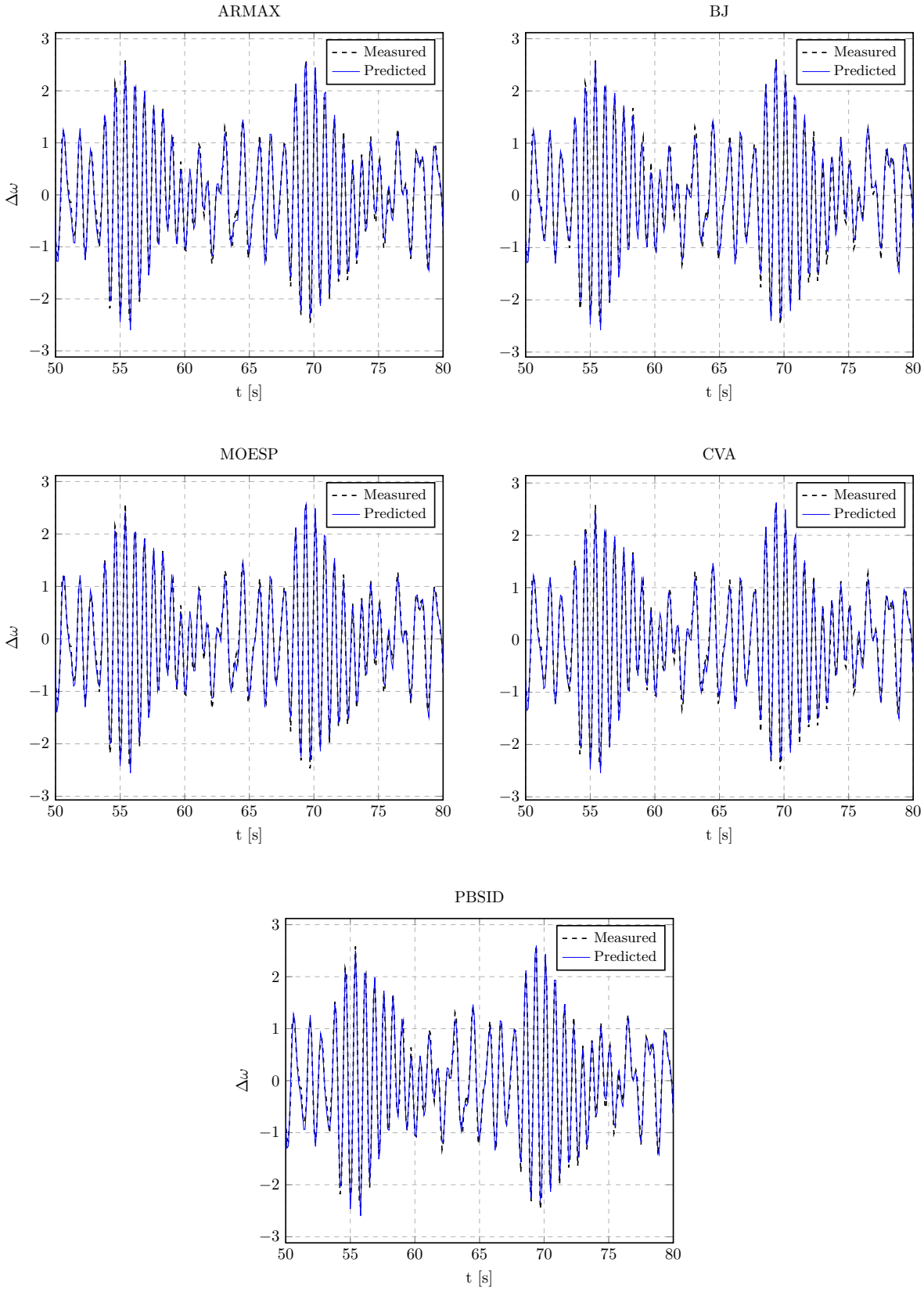

Figure 4.8: Predicted output of the identified system using various methods.

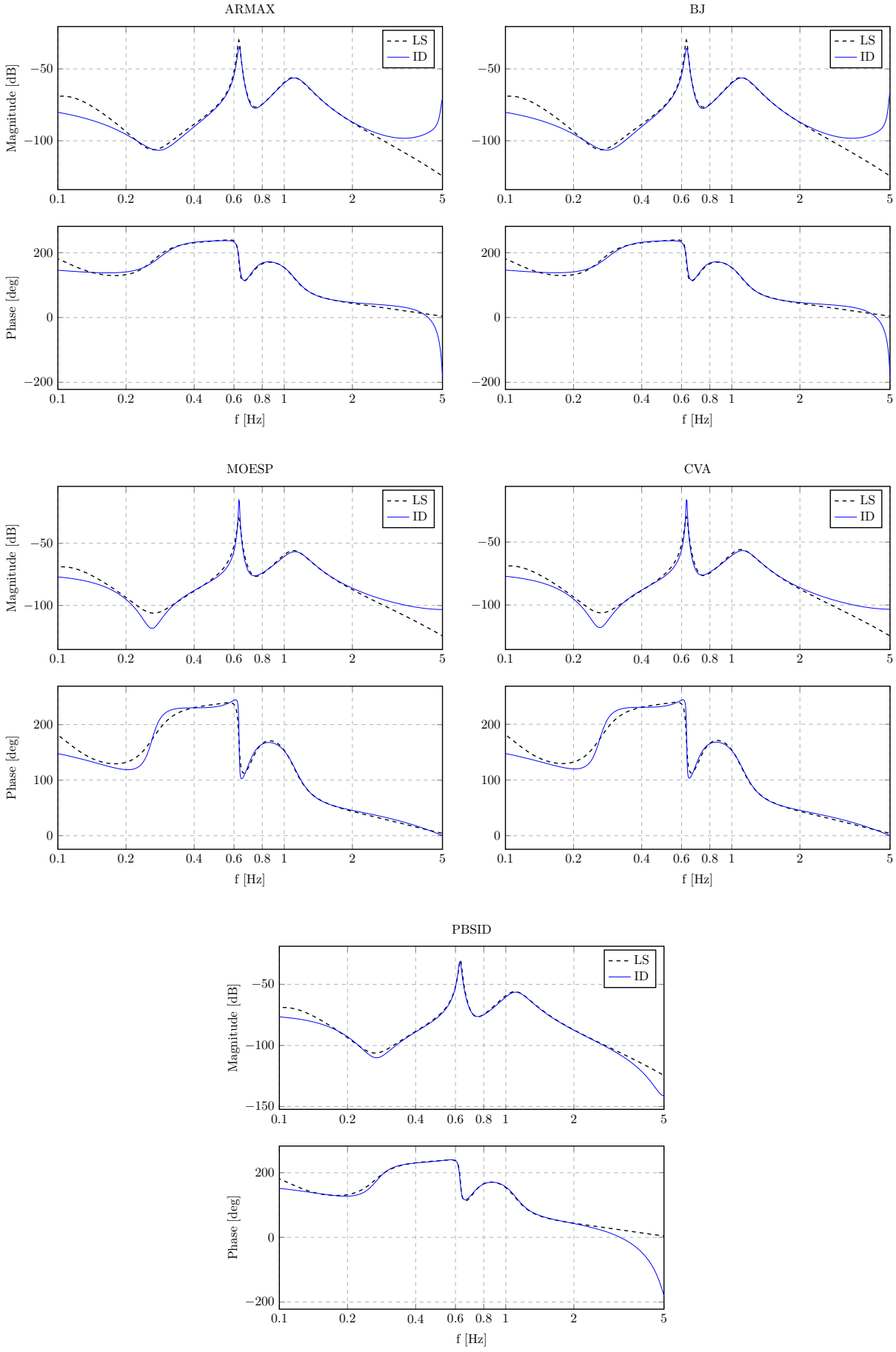

Figure 4.9: Frequency response of the identified system using various methods. (LS = Linearized system, ID = Identified system)

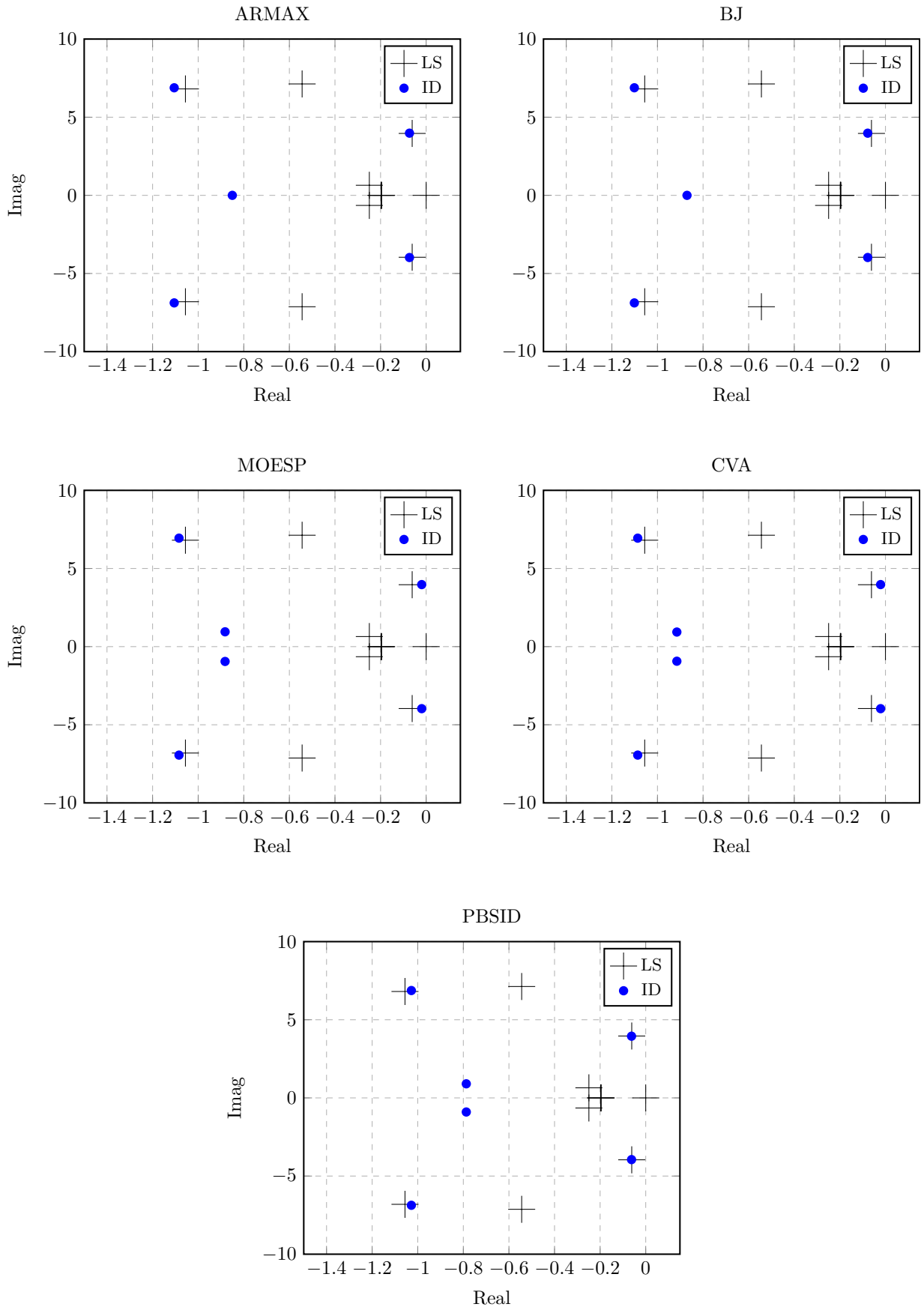

Figure 4.10: Eigenvalues of the identified system using various methods. (LS = Linearized system, ID = Identified system)

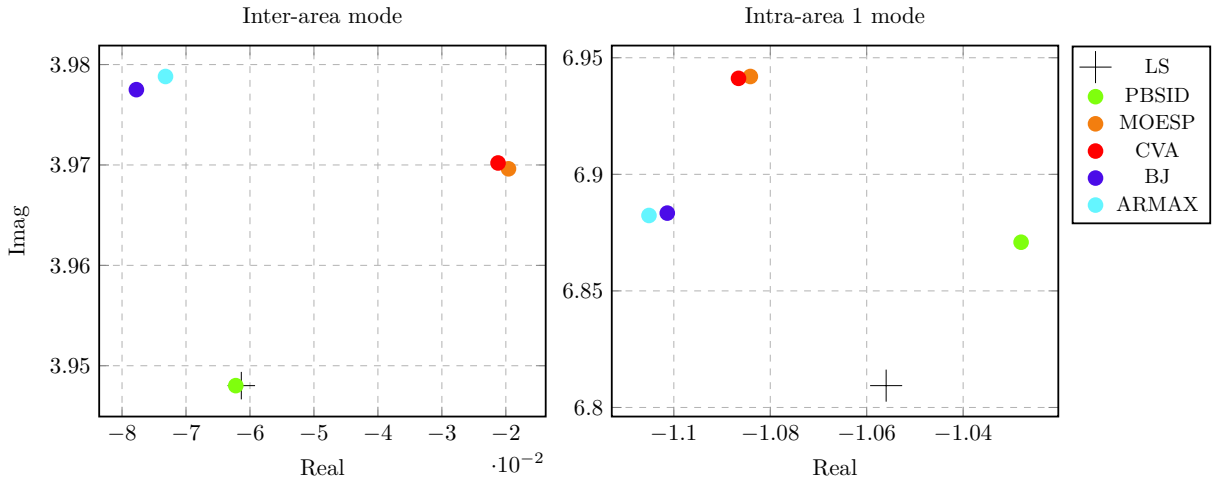

Figure 4.11: Zoom on the electromechanical oscillation eigenvalues of the identified system

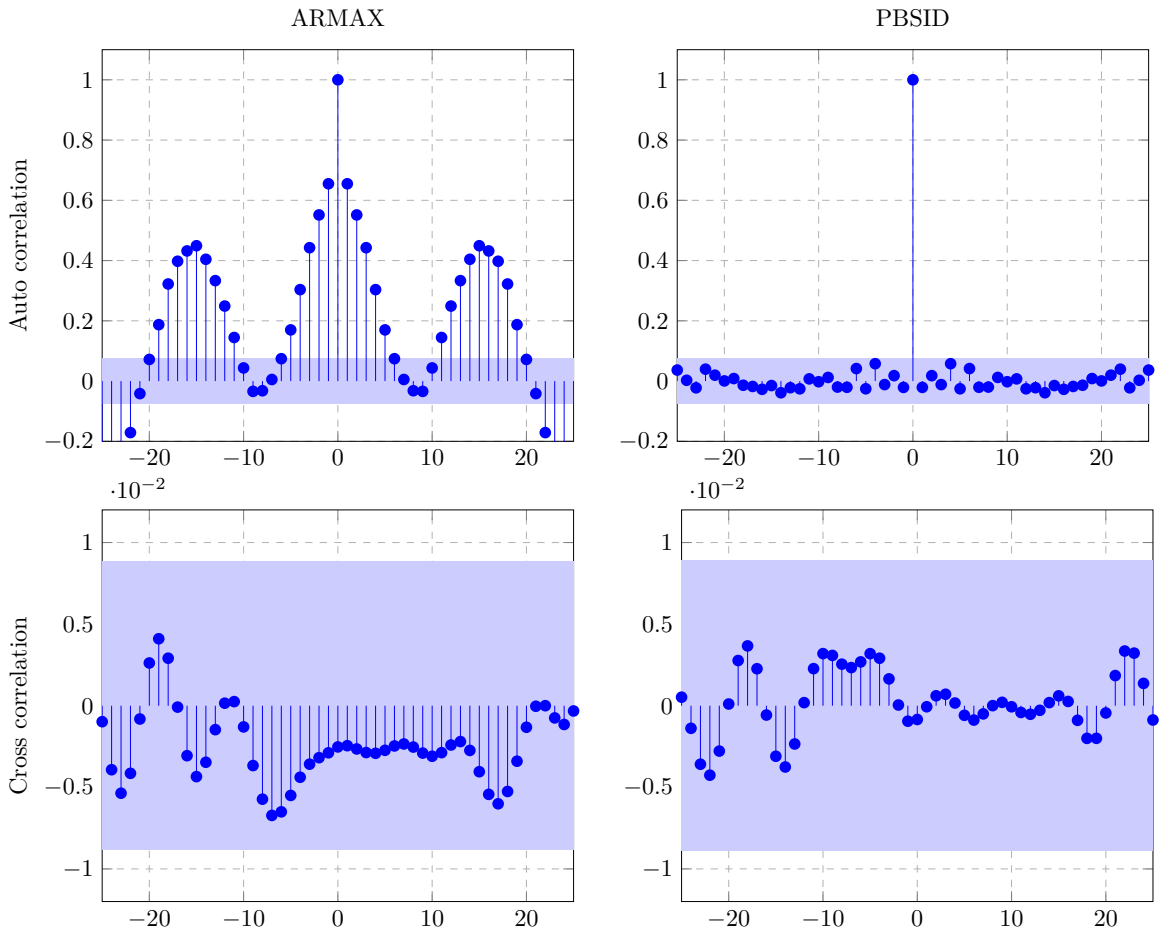

Figure 4.12: Residual test for ARMAX and PBSID.

Method	Order	ERR_y	ERR_{EIG}	ERR_ω
ARMAX	$[8, 7, 8, 1]$	0.1198	0.0181	0.4766
BJ	$[9, 6, 6, 9, 1]$	0.1201	0.0184	0.4748
MOESP	6	0.1302	0.0304	0.6737
CVA	6	0.1298	0.0300	0.6411
PBSID	8	0.1216	0.0132	0.4268

Table 4.2: System identification methods: order and performance. For BJ the order is referred to $[n_F, n_C, n_D, n_B, n_k]$ and for ARMAX to $[n_A, n_B, n_C, n_k]$

report the eigenvalues of all the simulations and in Fig. 4.13 and Fig. 4.14 we show the box plot of the low-frequency oscillation frequency and damping estimation error. For each method, we show the median error, the upper and lower quartile, and the maximum and minimum error. The compare the methods we have to look how much the median is closed to zero and how the error is spread around it. As expected CVA has again the worst accuracy, and PBSID has smaller error compared to ARMAX. In Fig. 4.16 we compare the frequency response and in Fig. 4.17 we show the box plot of the magnitude error. We can confirm that PBSID is the method with the best performance and in general the PEM method improves the accuracy of the accuracy of the estimation, but the PBSID itself gives good results and moreover it has lower computational complexity.

We conclude that PBSID, and eventuality an optimization with PEM, is the best method to obtain a low-order model of the power system between the ones we have considered in this thesis and it is the method that we will use in the next chapter to identify a model of the power system for the re-tuning of the PSSs.

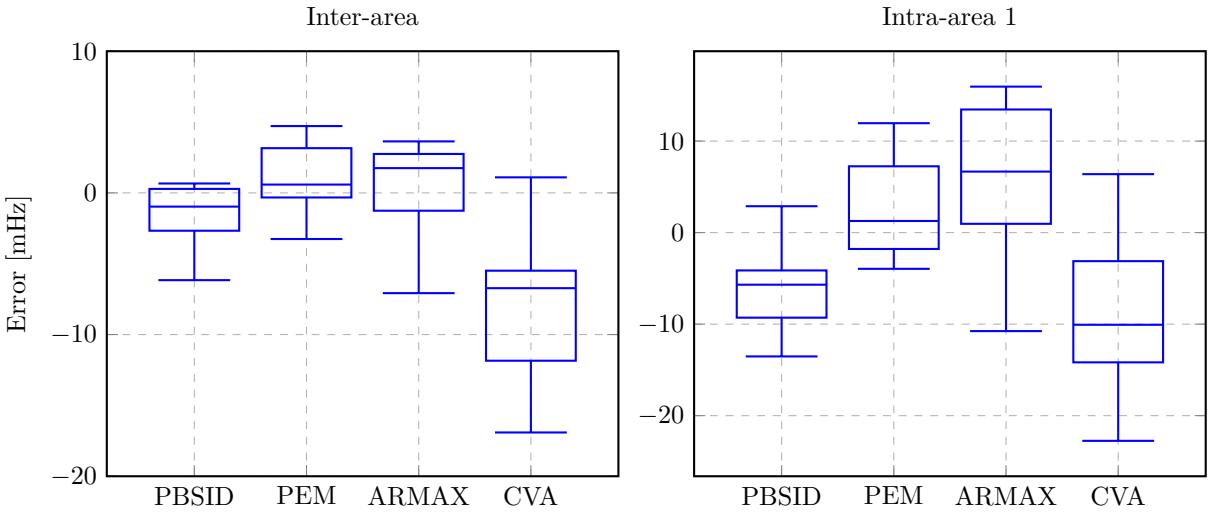

Figure 4.13: Box plot frequency error

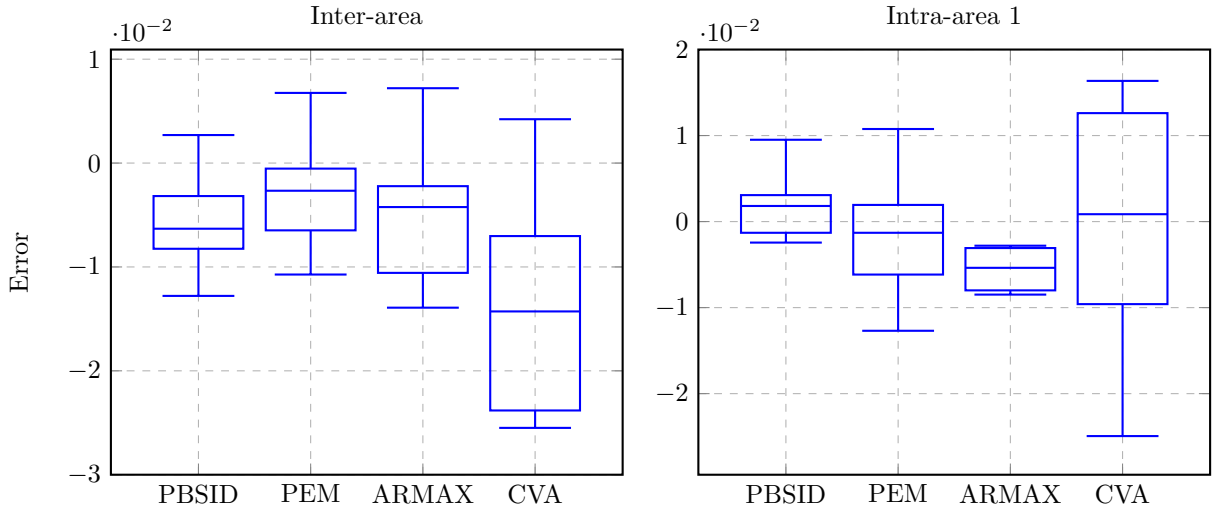

Figure 4.14: Box plot damping factor error

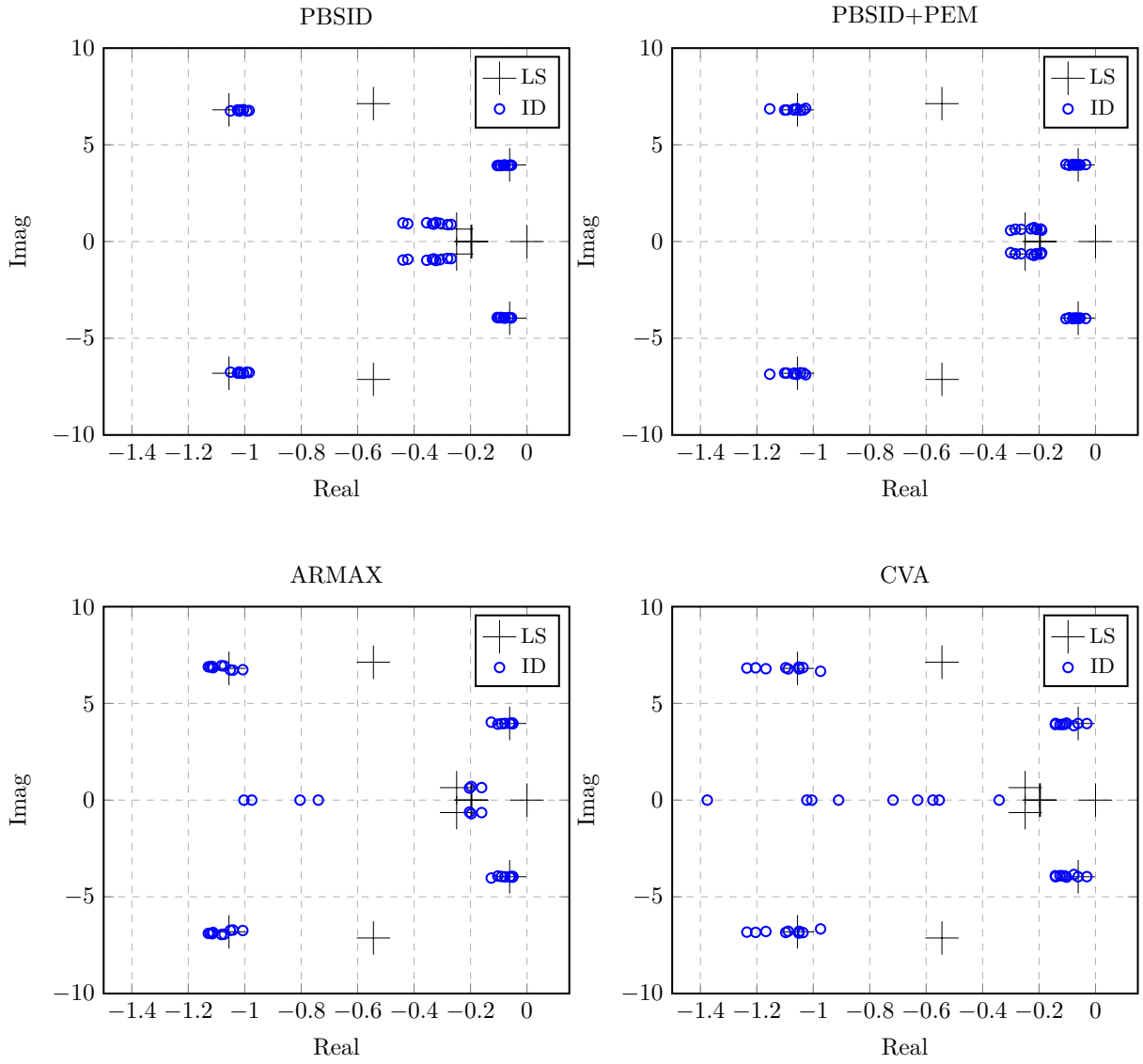

Figure 4.15: Eigenvalues of the identified systems from 50 simulations with different disturbance/noise realization

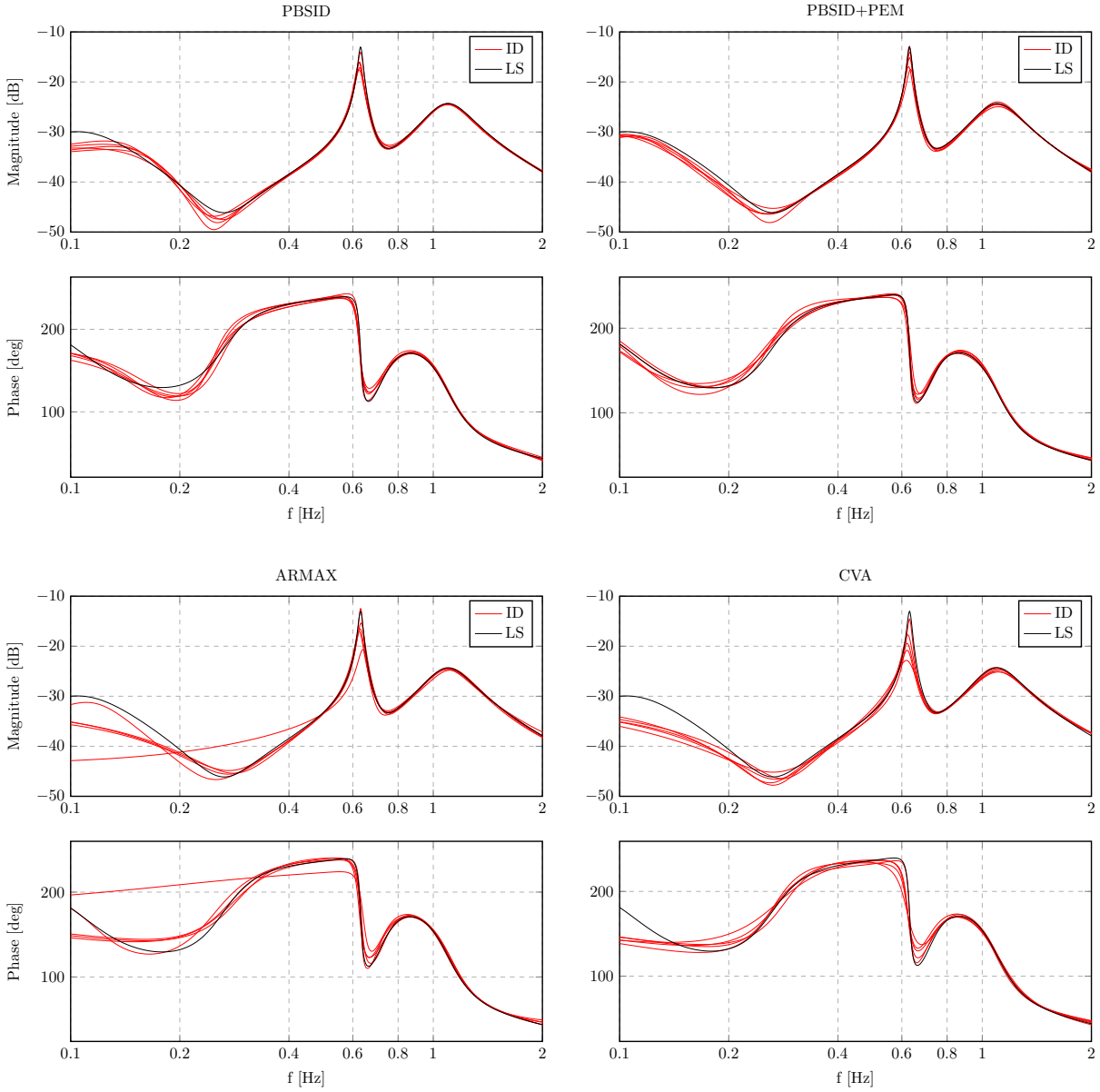

Figure 4.16: Frequency response of the identified system from 50 simulations. Only five cases are reported.

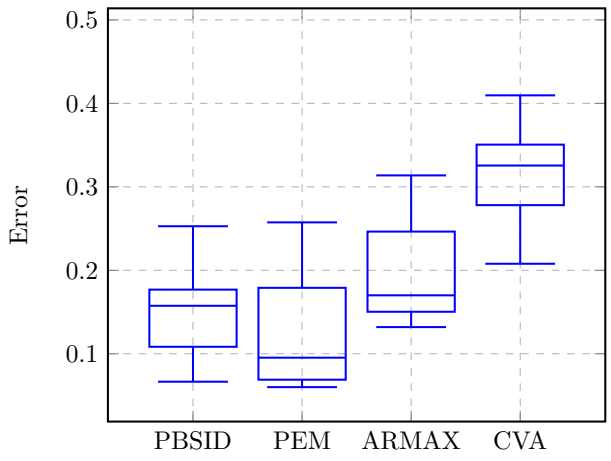

Figure 4.17: Box plot magnitude frequency response error

5

PSS tuning

In this chapter we illustrate the techniques used for the design of the Power System Stabilizers(PSSs). The design is based on the residue analysis and on the root locus methods. We applied the techniques to the identified low-order the power system model and we validate the method trough MATLAB simulations.

5.1 PSS Tuning based on residues and root locus

Consider the control diagram in Fig. 5.1, where $P(s)$ is the estimated model of the power system and $C_{PSS}(s)$ is the PSS transfer function as in (5.1) that includes only the gain and lead-lag blocks, meanwhile the washout block is included in $P(s)$.

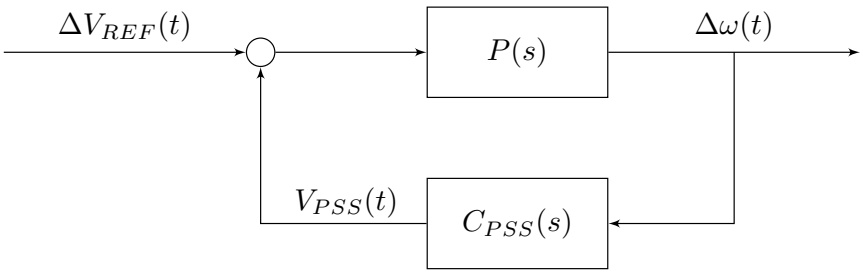

Figure 5.1: System control scheme

$$C_{PSS}(s) = K_{PSS}\,\frac{1+sT_1}{1+sT_2}\,\frac{1+sT_3}{1+sT_4} \tag{5.1}$$

The open-loop transfer function $P(s)$ can be expanded in partial fraction, as shown in (5.2). The residue R_i can be computed from the state-state representation (3.24) of the identified model as in (5.3), where $\mathbf{v}_i$ and $\mathbf{w}_i$ are respectively right and left eigenvector associated to the eigenvalue λ_i.

$$P(s) = \sum_{i=1}^{N} \frac{R_i}{s-\lambda_i} \tag{5.2}$$

$$R_i = \mathbf{C}\mathbf{v}_i\mathbf{w}_i^T\mathbf{B} \tag{5.3}$$

The residue gives the sensitivity of the associated eigenvalue to a static feedback and hence the direction in which the eigenvalue will move in the complex plane. Since our aim is to move the poorly damped eigenvalues to the left part of the complex plane, we have to tune the parameters of the PSS such that this happens. We select the least damped eigenvalue $\lambda^* = \sigma + i\omega$ and the PSS is designed for this specific eigenvalue. It can be shown [43] that the eigenvalue deviation is given by equation (5.4) and we can set the controller parameters to satisfy (5.5). That is equivalent to say that the controller has to introduce a phase compensation of ϕ degree at the frequency ω.

$$\Delta\lambda^* = R^* C_{PSS}(\lambda^*) \tag{5.4}$$

$$180^\circ = \angle R^* + \angle C_{PSS}(\lambda^*) \quad \text{or} \quad \angle C_{PSS}(\lambda^*) = 180^\circ - \angle R^* := \phi \tag{5.5}$$

Based on the required phase compensation we can select the time constants T_i of the lead-lag blocks and then the gain K_{PSS} to move the eigenvalue as much as possible to the left or to satisfy some other performance requirement. To design the time constants we simplify the transfer function of the PSS, as shown in (5.6), in which the two lead-lag blocks are identical.

$$C_{PSS}(s) = K_{PSS}\left(\frac{1+sT}{1+s\alpha T}\right)^2 \tag{5.6}$$

To select the time constant T and the constant α in (5.6), we use the formula in (5.7), that can be obtained by imposing the maximum phase shift in ω and such that the phase compensation in ω is exactly the angle ϕ.

$$\alpha = \frac{1-\sin\phi}{1+\sin\phi}, \quad T = \frac{1}{\omega\sqrt{\alpha}} \tag{5.7}$$

Instead, for the gain K_{PSS} we solve the optimization problem in (5.8), where we maximize the minimum damping factor over all the eigenvalues. This is done because the lead-lag blocks are designed for the most undampened mode and then it can happen that the other modes will move too far to the right and compromise the overall performance. Moreover, we add a regularization factor μK to avoid large gains as a solution.

$$K_{PSS} = \arg\max_K \left[\min_i \left(\xi_i(K)\right) - \mu K\right] \tag{5.8}$$

This problem does not have an analytic solution. However, we are not interested in the precise optimal solution but rather in a solution that satisfies the requirement. We compute the cost function $\min_i \left(\xi_i(K)\right) + \mu K$ for a finite set of gains and we select the one that maximises it. The algorithm is summarised in the Fig. 5.2.

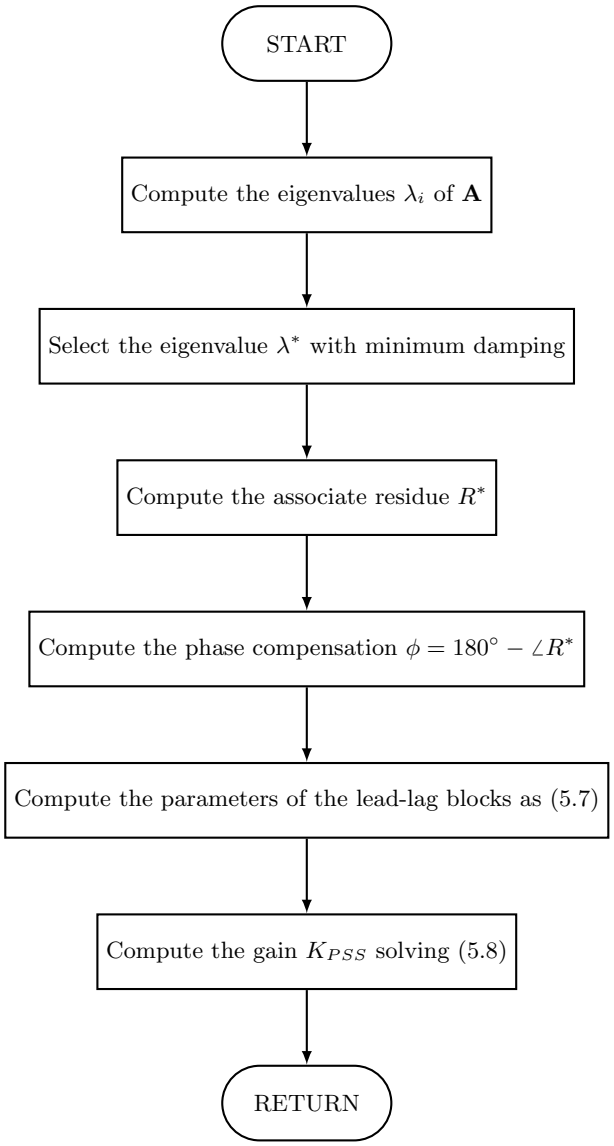

Figure 5.2: PSS design method flowchart

5.2 Validation

We consider the Two-Area Four-Generators power system described in Chapter 4. We suppose the PSS on generator 1 has to be retuned because the performance is not satisfactory.

We collect input-output data and we identify a low-order linear model with the PBSID method plus the PEM method to optimize the estimated model. We compute the low-frequency oscillation eigenvalues for the open-loop system which are reported in Table 5.1. We select the less damped mode that is $\lambda^* = -0.066 \pm 4.007i$ and we compute the parameters of the lead-lag blocks accordingly to equations (5.5) and (5.6).

In Fig. 5.3 is reported the root locus of the system with the phase compensation.

	Eigenvalue	Frequency [Hz]	Damping
Open-loop	$-0.066 \pm 4.007i$	0.64	1.62 %
	$-1.182 \pm 7.044i$	1.12	16.54 %
Closed-loop (Tuned)	$-0.443 \pm 4.115i$	0.65	10.70 %
	$-5.718 \pm 10.629i$	1.69	47.37 %
Closed-loop (Old)	$-0.173 \pm 4.177i$	0.66	4.14 %
	$-0.759 \pm 7.716i$	1.23	9.79 %

Table 5.1: Electromechanical modes of the Two-Area Four-Generators system in open-loop and in closed-loop with the old PSS and the tuned one (computed from the identified model)

	Eigenvalue	Frequency [Hz]	Damping
Closed-loop (Tuned)	$-0.405 \pm 4.062i$	0.65	9.91 %
	$-5.718 \pm 10.629i$	1.66	42.35 %
Closed-loop (Old)	$-0.161 \pm 4.119i$	0.66	3.89 %
	$-0.652 \pm 7.411i$	1.18	8.77 %

Table 5.2: Electromechanical modes of the Two-Area Four-Generators system in open-loop and in closed-loop with the old PSS and the tuned one (computed by linearizing the system)

For a small gain, the selected eigenvalue, highlighted in red, is moving horizontally to the left increasing the damping factor. In the figure are reported also the 10% damping bounds. That it is the performance requirement that the design has to satisfy.

Then, we compute the cost function in (5.8) with $\mu = 0.1$ for K varying from 0 to 50 with a step of one. The optimal value is $K = 37$. In Fig. 5.3 and in Table 5.1 we report the new eigenvalues of the closed loop system with the tuned PSS. We can see that the less damped eigenvalue is moved inside the region with damping coefficient larger than 10% but also all the others eigenvalues are still in that region. For comparison, in Table 5.2 we report the eigenvalues of the closed-loop system obtained from the linearization of the system. Despite the small differences between the eigenvalues obtained from the identified system and the one obtained from the linearization, we can increase the overall performance of the system through the re-tuning of the PSS.

Finally, to validate the methods, we simulate the power system in Matlab using the Power System Toolbox. To excite the dynamic and the oscillations we simulate a three phase to ground fault at bus 8 and the disconnection of the lines between bus 7 and 9 after 0.05 seconds. In Fig. 5.4 are reported the rotor speed of the first generator and the tie-line power evolution without the PSS, with the badly tuned PSS and with the one tuned with the proposed method. As expected, without the PSS the system presents badly damped oscillations. With the old PSS the oscillations are more damped but after 20s they are still present. Meanwhile, with the tuned PSS they almost disappear after

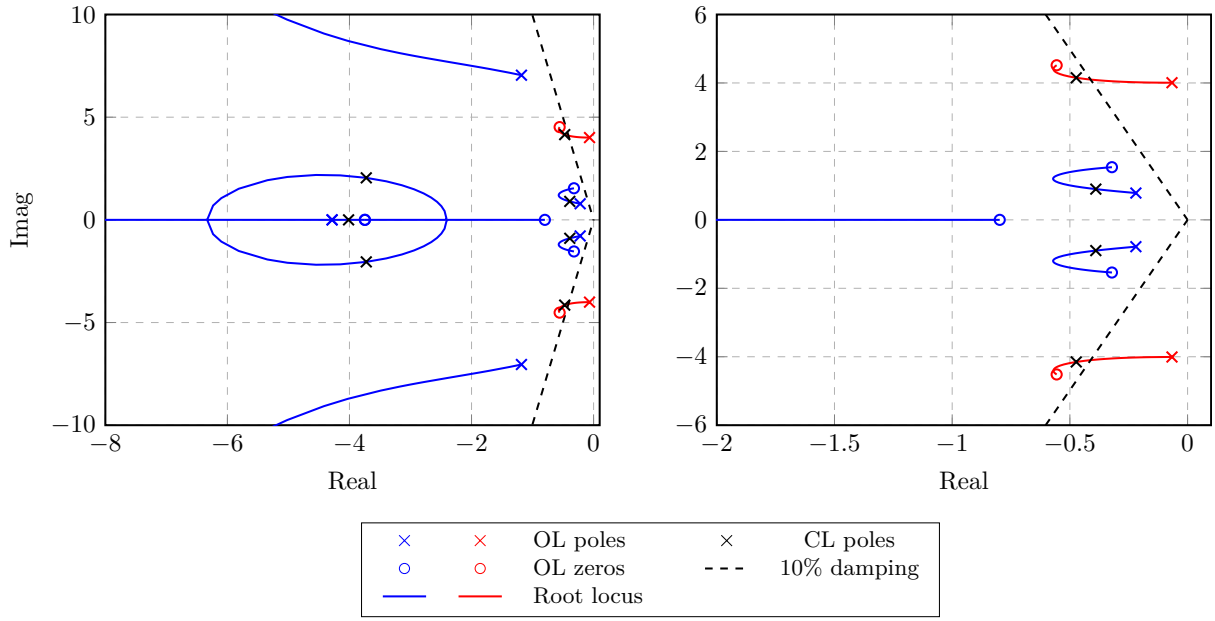

Figure 5.3: Root locus of the system with phase compensation. The root locus of the eigenvalue with minimum damping is highlighted in red. The right plot is the zoomed version of the left one.

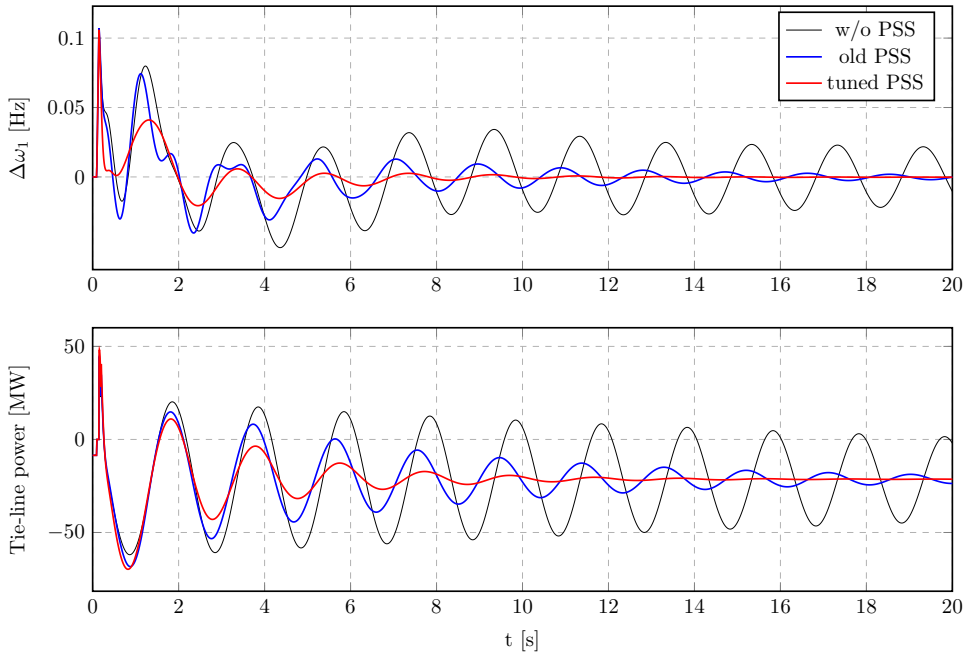

Figure 5.4: Fault simulation w/o PSS, with the improperly tuned PSS and with the tuned one

10s.

We can conclude that the low-order model identified with the PBSID method and then optimized with the PEM method is adequate for the tuning of the PSSs parameters and the technique based on the residue and root locus can be used to compute the parameters that guarantee the desired performance.

6

Real-Time Validation

In this chapter, we report the real-time validation of the method proposed for the identification of a low-order linear model of a power system to be used for the PSSs tuning. In the first section we briefly present Hypersim, the simulation software, that we used for the validation. In the next sections, we first report the validation that was carried out using the Two-Area Four-Generator system, presented also in the previous chapters. Then we approach a larger system, namely the New England 68-Bus System.

6.1 Validation framework

Hypersim by OPAL-RT is a high-performance simulator software for power systems. It has a rich library of components that can be used to model power grids. We used this software to perform the real-time validation of the proposed methods.
In Hypersim we design the power system models in our local PC, which is connected via the local network to the external high-performance machine, the OPAL-RT OP 5700, where the real-time simulation is processed. From Hypersim we can run and stop the simulation, and acquire the needed measurements. Moreover, a peculiarity of Hypersim is that we can change the parameters of the model during the running simulation. This has been very useful because we can modify online the parameters of the PSSs without stopping and restart the simulation.
Hypersim also has a Python API that has been used to manage and coordinate the simulation flow trough a Python script. Finally, since the scripts for the system identification has been developed in Matlab, we used the API Matlab Engine for Python to call the Matlab functions and process the data acquired from Hypersim.
The resuming diagram of the simulation framework is shown in Fig. 6.1.

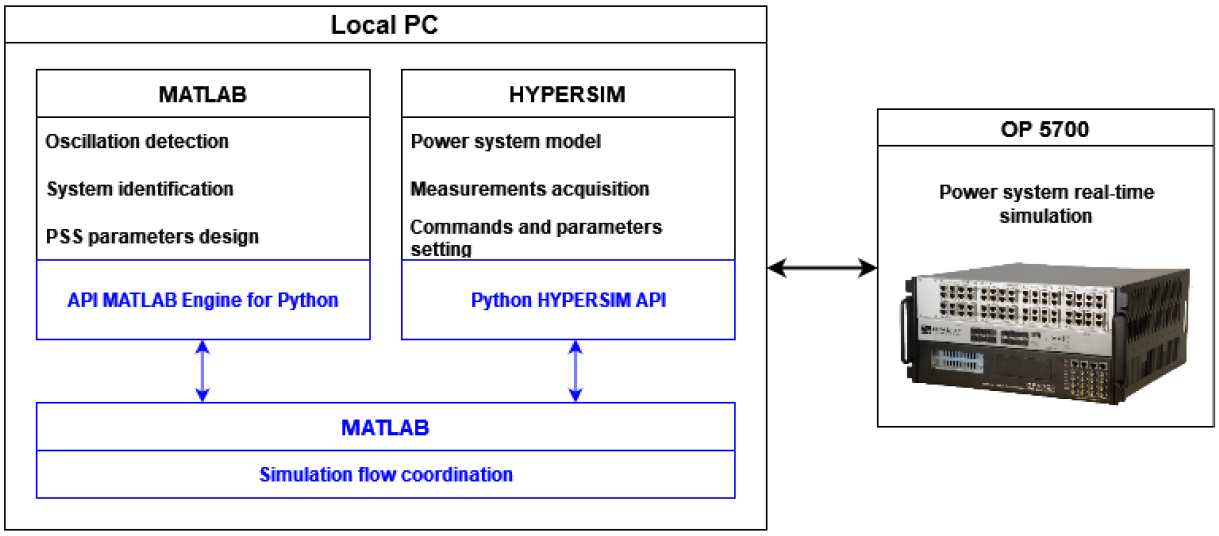

Figure 6.1: Simulation framework

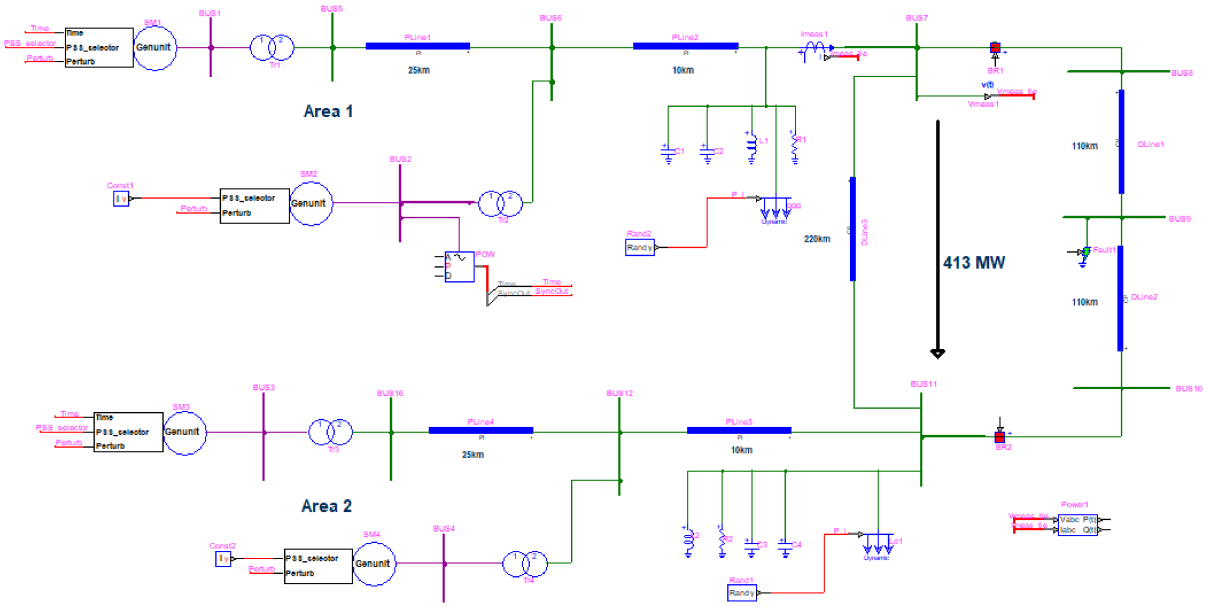

Figure 6.2: 2A4G, Hypersim model diagram

6.2 Two-Area Four-Generator system (2A4G)

Consider the Two-Area Four-Generator system presented in Chapter 4, whose Hypersim diagram is shown in Fig. 6.2. The validation scenario is the following: we suppose the PSSs installed at generators 1 and 3 are not properly tuned and there are improperly damped oscillations in the system. From ambient data, we can detect if there is any oscillation that is not dampened and activate the PSSs retuning procedure for the two machines. For each PSSs we identified a model by exciting the system with the probing signal, as described in Chapter 4. Then we used each model to tune the respective PSS.

In Fig 6.3, we show the time evolution of the speed deviation of G1 and G3. After

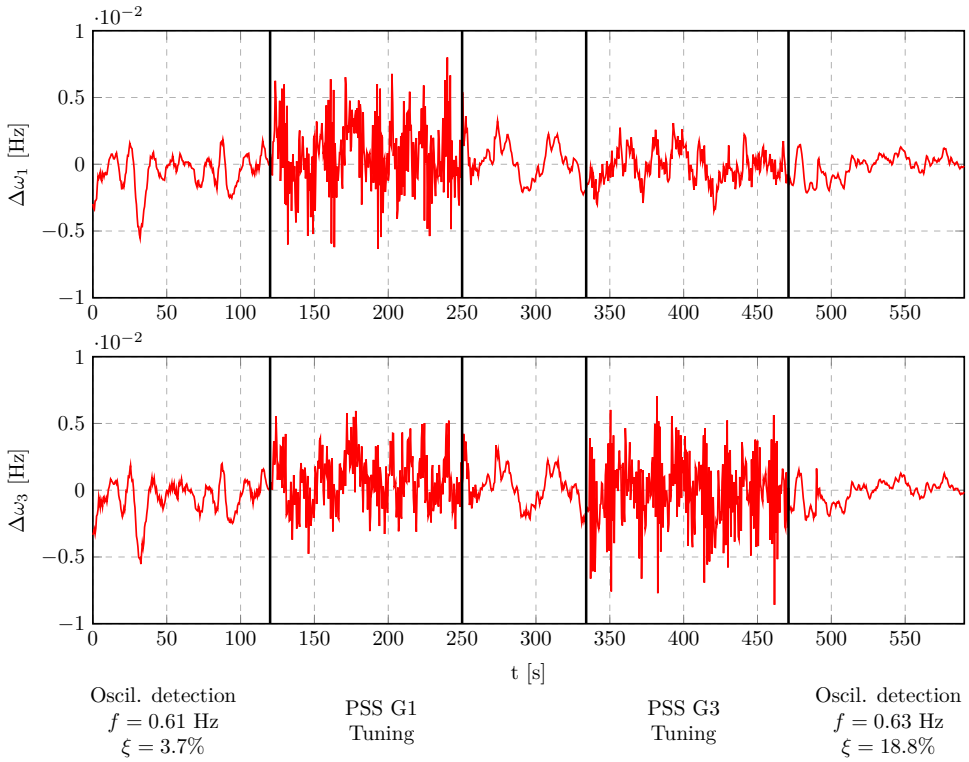

Figure 6.3: 2A4G - Simulation for PSSs retuning

starting the simulation, we collect 60s of ambient data recording the two rotor speed deviations. This is used to analyse the oscillations in the system.

If an undamped mode is detected in the ambient data, we activate the excitation signal and we record for 120s the input-output data to identify the low-order model seen from generator 1. We compute the new parameters for the PSS and we update them in the running simulation. Afterwords, we do the same for generator 3. Finally, we analyse 60s of ambient data to see if we have improved the overall damping.

Before the tuning of the PSSs there is a mode at frequency $f = 0.61\,\text{Hz}$ with a damping factor of $\xi = 3.7\%$. This means that the stability margin is small and changes in the power system may bring the system into an unstable configuration. After the retuning, the least damped mode is at frequency $f = 0.63\,\text{Hz}$ but we have increased the damping to $\xi = 18.8\%$.

Notice that the perturbation introduced by the probing signals during the identification is comparable with the natural load variation meaning that low-level probing signals can be used effectively to identify a model of the power system.

The frequency response of the identified model for generator 1 and 3 are reported in Fig. 6.4. Unfortunately, from the Hypersim model we are not able to extract a linear model of the system to validate the identified model. Hence, we resort to the residual analysis to approve or reject the model. In Fig. 6.5 we show the root locus used to design the PSS parameters, where we compare the eigenvalues before and after the retuning. In Table 6.1 we report the PSSs parameters.

In Fig, 6.6 we show the response of the power system after a three-phase to ground

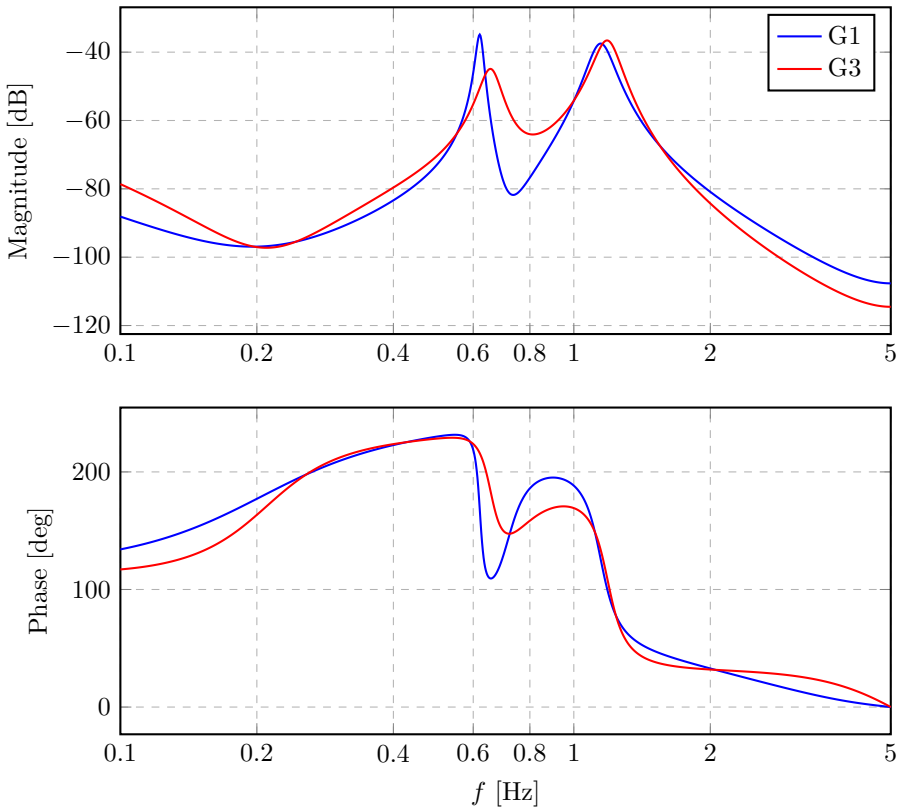

Figure 6.4: 2A4G - Frequency response of the identified models

Generator	PSS	K_{PSS}	T_1, T_3 [s]	T_2, T_4 [s]
G1	Old	10	0.080	0.015
	Tuned	32	0.290	0.222
G3	Old	10	0.080	0.015
	Tuned	28	0.238	0.240

Table 6.1: 2A4G - PSSs parameters

fault at bus 8 and the disconnection of the line between bus 7 and 9 after 0.05 seconds to isolate the fault. Moreover, we show also the re-connection of the line after the clearing of the fault. From both cases we can see that after the retuning of the PSSs we have overall better performance with regard to the oscillation damping. From tie-line power evolution, we can see how the oscillation are much more damped. In particular, in the re-connection of the line, with the old PSSs the oscillation lasts for $20 - 25$s meanwhile, after the retuning they disappear after only 10s. Moreover, we can see that we can remarkably reduce the frequency deviation peaks of the two generators.

We can conclude that the proposed method works as expected also online in real-time simulations and it can be applied online during the normal activity of the power system.

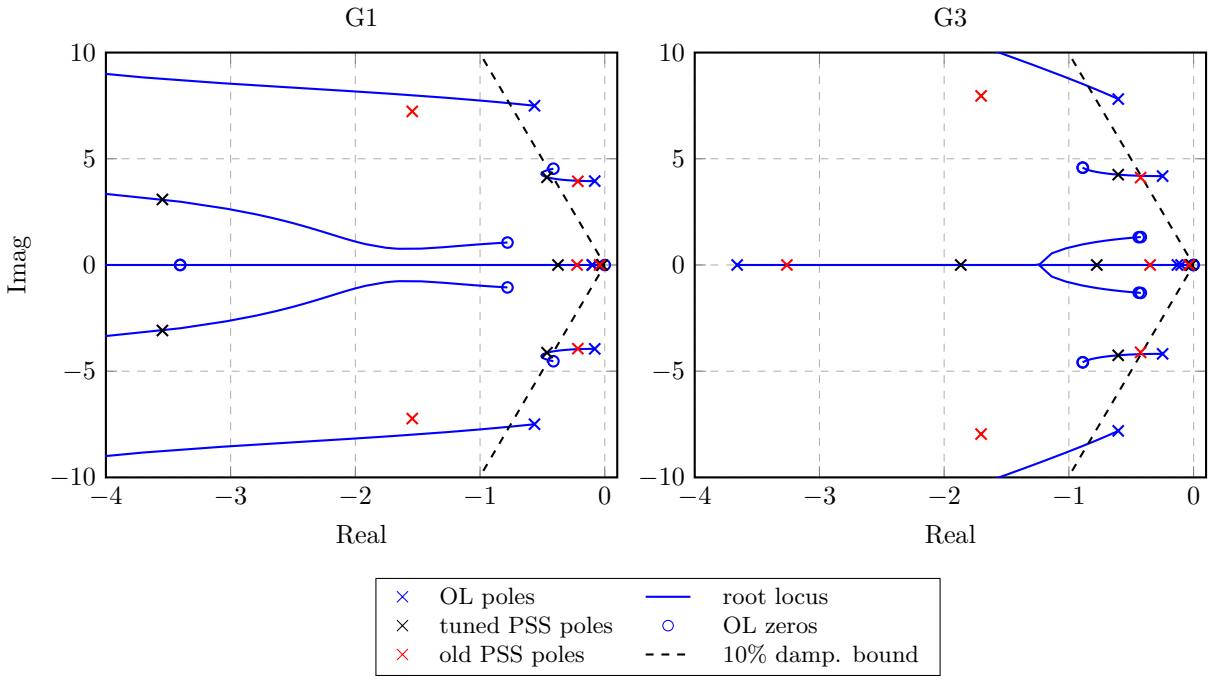

Figure 6.5: 2A4G - Root locus for PSSs retuning

6.3 New England 68-Bus system (NE)

To validate the proposed method in a more complex power system, we consider the New England 68-Bus test system [44]. We used this model because is one of the standard system used for oscillation analysis and PSS tuning test. The data of the model can be downloaded from [45] in PSS/E format ans then imported in Hypersim. However, in order to obtain a model with which one can work, the model diagram has to be manually routed. In Fig. 6.7 and in Fig. 6.8 we show the power system diagram. It is composed of 16 synchronous generators, 68 buses and 35 loads. Ir represent a reduced order equivalent model of the New England test system (containing G1 to G9) interconnected to the New York power system (containing G10 to G13). In the original model the generators G14, G15 and G16 represent the connection to the neighboring areas. Meanwhile, in this work they are treated as standard generators. Each machine is equipped with the TGOV1 governor/turbine system model and with the SCRX excitation system. Its model is equivalent to the Simple Exciter model presented in Chapter 2 but also has negative current logic circuit at the output. However, it can be disabled.

6.3.1 Scenario 1: Retuning of PSSs

The first validation scenario that we have carried out is to see if the proposed algorithm can work also in this more complex system. Suppose the PSS at generators 3 and 13 are not properly tuned (we set manually bad parameters) and we try to tune them to improve the performance. As done previously, we excite the system through

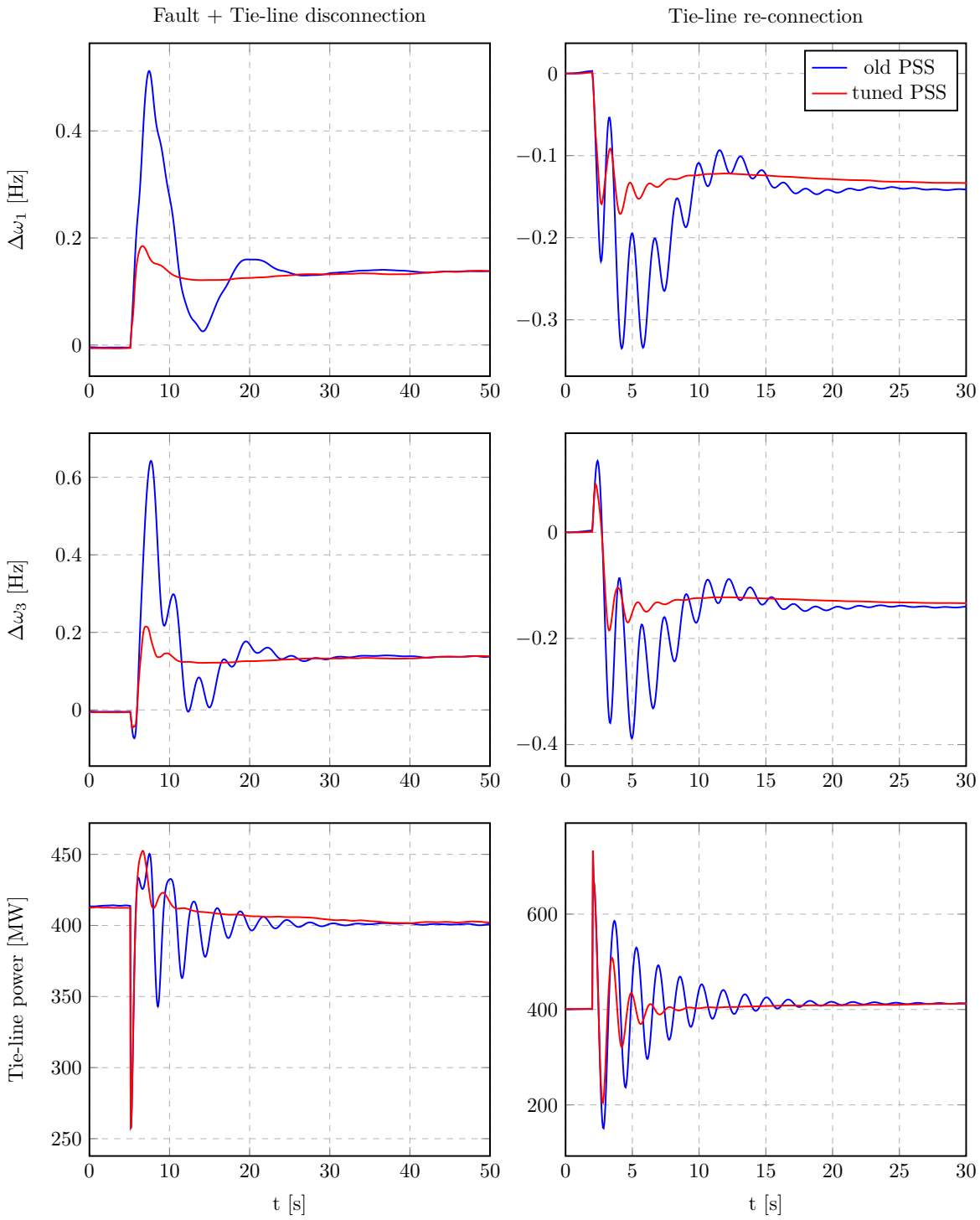

Figure 6.6: 2A4G - Faults simulation comparison

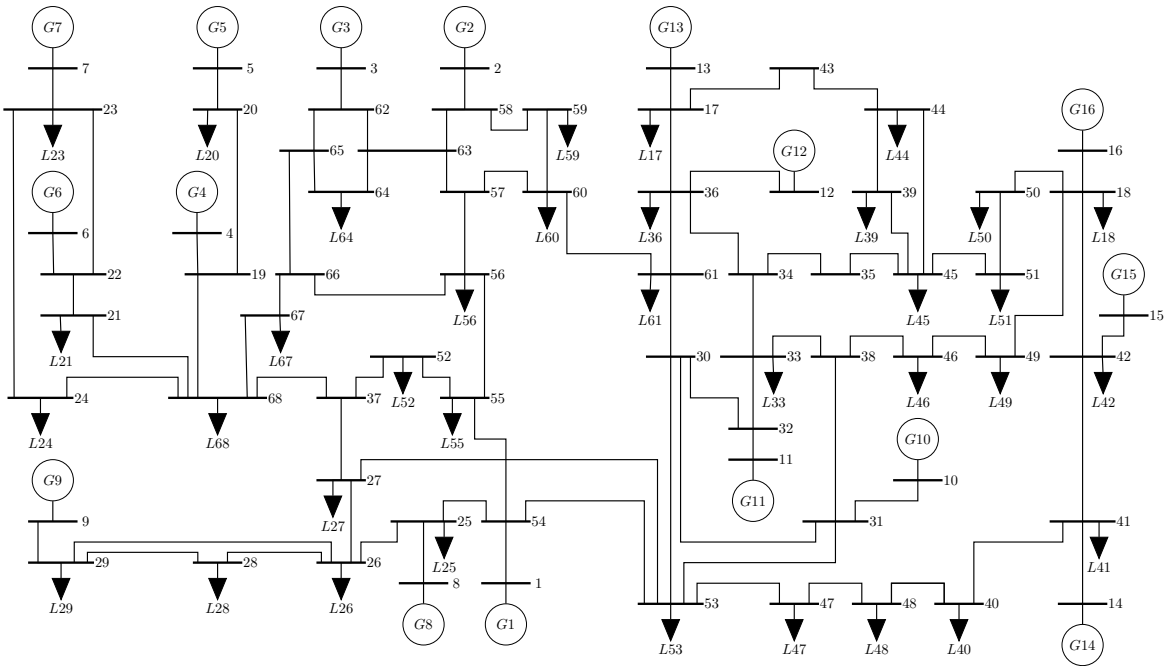

Figure 6.7: New England power system diagram

the probing signals and we collect the input-output data to identify a low-order model of the system. In Fig. 6.9 is reported the Bode plot of the identified model for the two generators. Meanwhile, in Fig. 6.10 the root locus used to design the controllers is shown. The two models present different oscillation modes. In particular, generator 3 (G3) is involved in three oscillation modes. The higher frequency mode is slightly observable, there is almost a zero-pole cancellation, and is also not controllable, since through the feedback we cannot move it. This eigenvalue could be a actual mode of the system or just an artefact introduced in the identification to fit the data. Moreover, we have to pay particular attention when we design the gain of the PSS. Following the procedure in which we maximize the damping, this eigenvalue will limit the gain since we can not move it. To solve this problem, the gain can be set manually by looking at the root locus or this particular eigenvalue could be excluded from the object function when we maximize the damping. The model presents two other oscillation modes. One has large controllability and we can increase considerably the damping by moving it. The other one at a lower frequency, has less controllability. However, we can bring it inside the 10% damping region. From experience, the first one is related to a local mode, instead, the second probably is related to an intra- or inter-area mode and to increase the damping we also have to act, i.e. retune the PSS, on the other machines involved in this mode.
For generator 13 (G13), instead, the model has only one mode that is not adequately dampened, but through re-tuning, we can increase the damping even if we can not reach the 10% bound. Also for this mode, we can expect it to be an intra/inter area mode and we have to act also on the other machines.

Finally, to validate the methods we look at the transient response of the system after

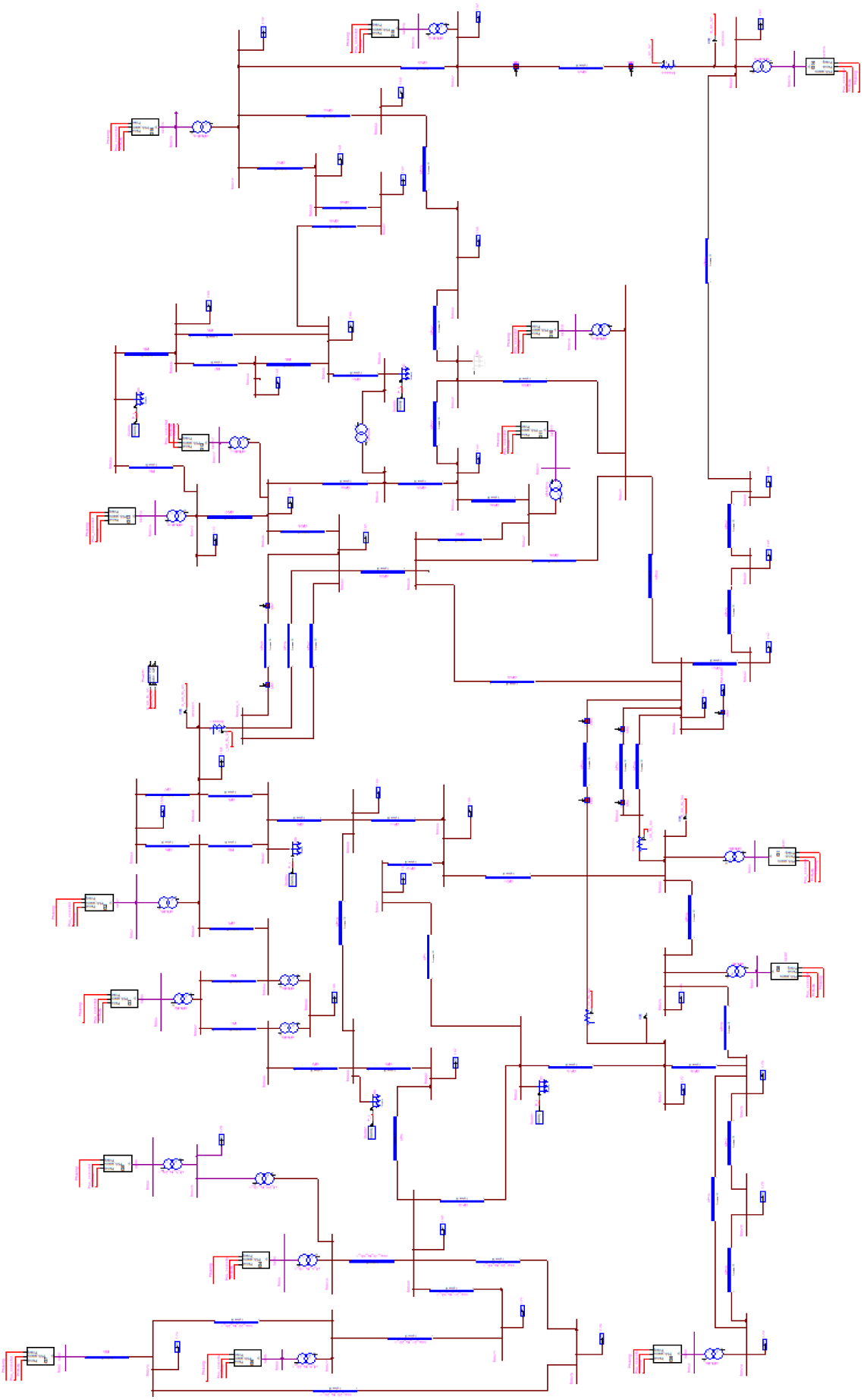

Figure 6.8: NE - Hypersim model diagram

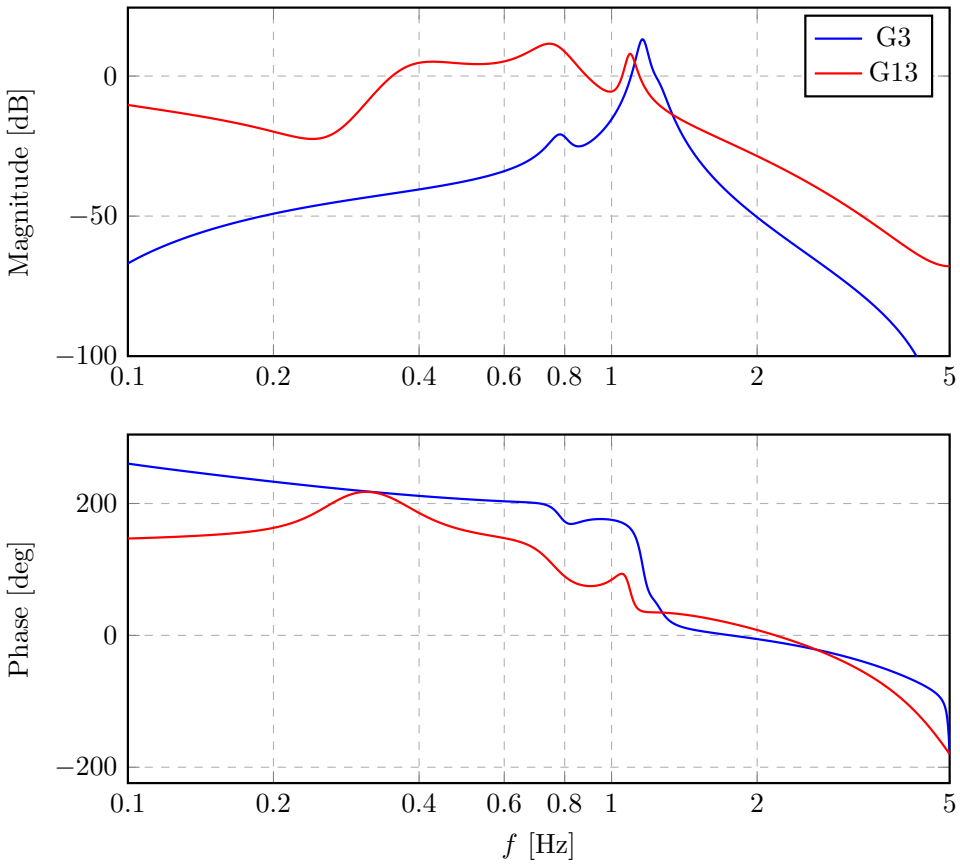

Figure 6.9: NE - Validation scenario 1 - Bode plot of the identified models

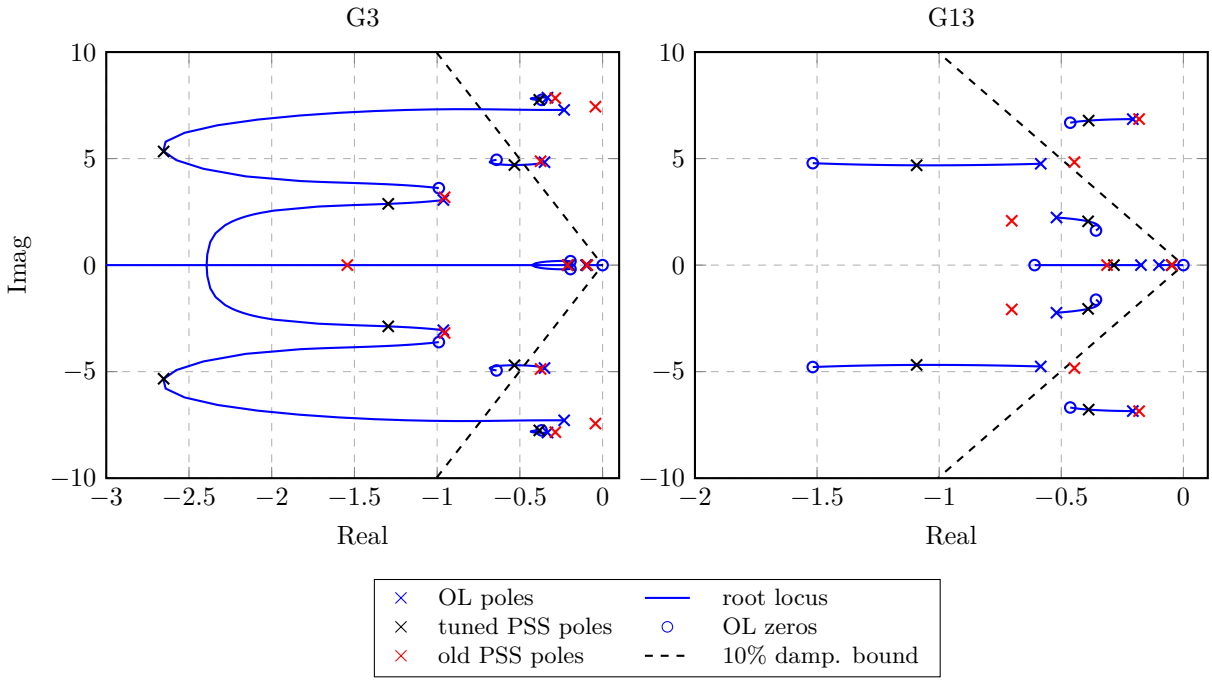

Figure 6.10: NE - Validation scenario 1 - Root locus

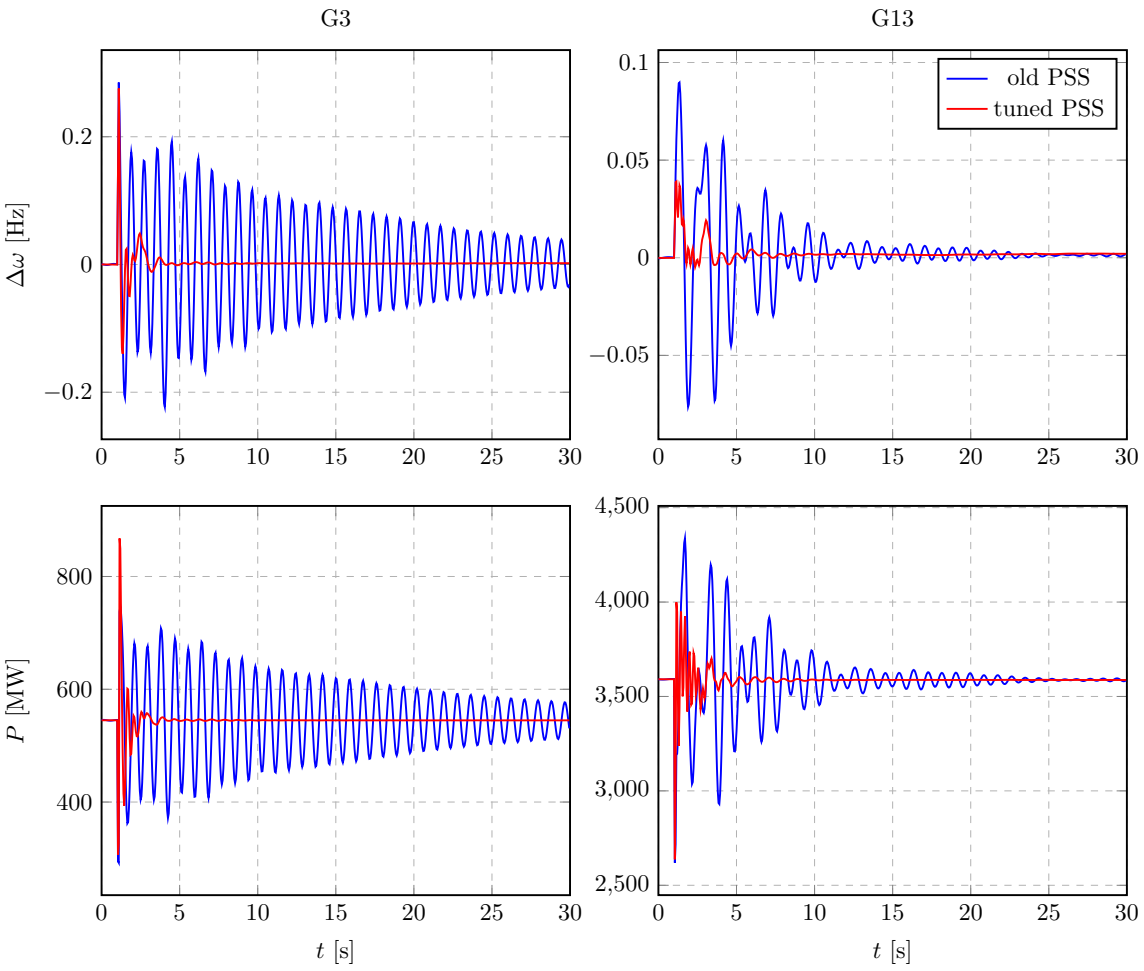

Figure 6.11: NE - Validation scenario 1 - Fault simulation with the improperly tuned PSSs and with the tuned one

a fault, shown in Fig. 6.11. The fault is a three-phases to ground fault at bus 60. We can conclude that also with more a complex model, the proposed method can identify a correct model that can be used to design the parameters of the PSSs and the new controller can improve the damping of the low-frequency oscillations.

6.3.2 Scenario 2: increasing in renewable generation

We build a scenario in which we present a real use case of the proposed method in which we show that the retuning of the PSSs can save the power system from instability when the configuration changes. In particular, we add several PQ generator buses in the model to simulate the integration of renewable sources. The power rating of the generators and the added PQ buses are listed in Table 6.2.

Generator 16 is the swing bus and the power is given by the load flow solution. We have three configurations: initial, tuning and final. We suppose that the PSSs are properly tuned for the initial configuration. Then bring the system to the final configuration by increasing the power of the PQ buses and decreasing the one of the generators until reaching the final configuration. In this new configuration the system

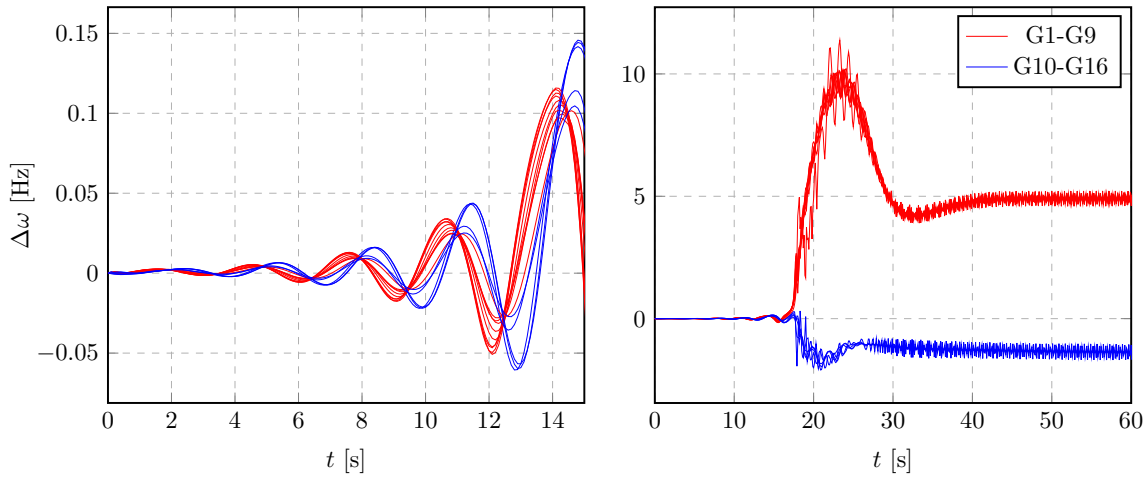

Figure 6.12: NE - Validation scenario 2 - Oscillation divergence at final configuration

becomes unstable: starting from the equilibrium point given by the load flow solution, the system starts to oscillate until we lose the synchronization between the group of generators 1-9 and the group 10-16, as shown in Fig 6.12.

Instead, if during the increasing of the PQ power when we reach the tuning configuration, we re-tune the PSSs in generators 3, 6, 9, 14, 15 we can maintain the power system in a stable configuration. The general idea is to be able to detect the reduction of the stability margin and the need to retune the PSSs using the ambient data. In our case, we are not able to estimate correctly the modes of the system. The problem with a larger system is a large number of modes that makes the estimation more difficult and also it is harder to understand in which machine one has to retune the PSS. Since the mode estimation from ambient data is not the main focus of this work, we did not dig into it. The tuning configuration was chosen manually setting the added PQ buses power to the 85% with respect to the final configuration. Also the generators where retuning the PSS were chosen manually. After having identify a model for each of them, we selected the one with modes closed to be unstable.

To see the behaviour of the system in the final configuration with the PSSs tuned in the tuning configuration, we simulate the disconnection of a 50 MW load at bus 53. The result of the simulation are shown in Fig. 6.13. We can see that the oscillations do not diverge and the retuning can guarantee good performance also in the final configuration. The frequency deviations are not diverging, they converging towards steady state value. Since the system in general is slow to compensate load variations, it takes more than the 20s plotted in the figure to reach the steady state.

In conclusion, we validated the proposed method in two different models. In the first model, namely the Two-Area Four-Generator system, we validated the applicability of the method in real-time simulation and tested the entire chain: oscillation detection, model identification, PSSs returning, oscillation damping check. The method for identification and PSS retunig works as expected, we are able to identify a proper model

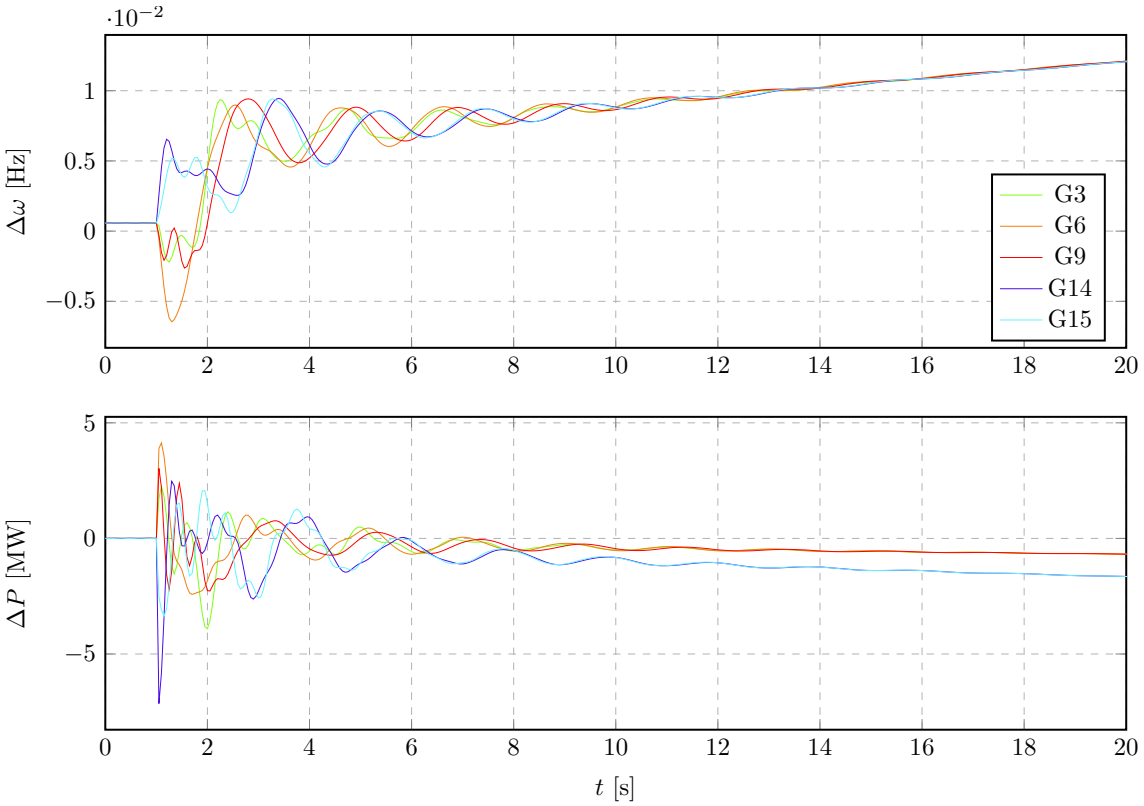

Figure 6.13: NE - Validation scenario 2 - using the final configuration of the generators and added PQ buses, but after retuning of PSSs in G3, G6, G9, G14, G15.

and to retune the PSSs to satisfy the required performance. Therefore, we are confident that it can also be used in a real system. In the second model, namely New England 68-Bus system, we tested our solution in a larger model. Despite the higher complexity, the proposed method is capable of increasing the system performance. Finally, we present a use case in which we show that the retuning of the PSSs based on system identification can prevent the system from becoming unstable.

	Power [MW]		
	Initial	Tuning	Final
G1	140	128	117
G2	508	466	424
G3	519	476	433
G4	614	563	512
G5	292	268	244
G6	546	500	455
G7	600	550	500
G8	463	424	386
G9	560	513	467
G10	624	572	520
G11	1186	1087	989
G12	735	674	613
G13	4309	3950	3591
G14	1302	1195	1085
G15	1200	1100	1000
G16	-	-	-
BUS19	254	432	509
BUS22	303	515	606
BUS24	155	264	301
BUS28	446	768	892
BUS64	507	861	1014
BUS68	468	795	936

Table 6.2: NE - Validation scenario 2 - Generation power for generators and added PQ buses in the initial, tuning and final configuration.

7

Conclusions and Future Work

In this chapter we summarise the work of the thesis and we present some possible future work.

7.1 Conclusions

In this thesis, we presented a framework for online automatic tuning of PSS based on the identification of power system model. Note that the entire procedure can be performed without disabling the PSS. In this regard, while keeping the PSS online, the system identification is done in closed-loop. This generally makes identification more complicated. For this reason, several methods were compared in order to identify the most suitable one. The method with the best performance was the PBSID method, which identifies the model in state space. In addition, it can be further optimised using the PEM method, if necessary.

For the PSS tuning, a method based on residuals and root locus was used. Specifically, from the identified model, the eigenvalue with the lowest damping is selected and its residual is computed. From it, the parameters of the lead-lag blocks can be derived. Subsequently, the gain is calculated by maximising the minimum damping among all eigenvalues.

After developing and testing the methods in Matlab, we validated the entire procedure in real-time simulation, using Hypersym. Two different systems were considered: the Two-Area Four-Generator System and the New England 68-bus test system. In the first case, we validated the entire process in which the retuning procedure is triggered by detecting the presense of low-frequency oscillation from the ambient data. In the second, we validated the proposed method in a more complex system and then demonstrated through simulations how retuning of PSSs can save the system from instability. In both cases, we were able to identify a model of the system and re-tune the PSSs to increase the system damping performance. Therefore, we think that the proposed

method can be applied and improve the ability of power system operators to control the power system even in critical situations.

7.2 Future work

The work developed in this paper can be further developed in several directions. Some of them are reported in the following paragraphs.

Input selection and SNR analysis A proper selection of the input is important for the correct identification of the system. In this thesis, we use a multi-sine signal because we considered it was the most appropriate for our scope. Nevertheless, one can further investigate the role of the input and understand if there is a better choice.
Moreover, we did not dwell on the time window length of the recorded data. That can be further investigated together with its relation with the Signal-to-Noise Ratio (SNR). In general, we expect that the smaller the SNR (i.e., bigger impact of noise and disturbances on data quality) the more data we need for the correct model identification.

Field tests From real-time simulations, we think that the proposed method can also be directly applied in a real electrical power system. Field tests should be carried out to fully validate the method and assess its applicability.

Different PSS structure and different tuning methods In this work, we considered a simple structure for the PSS with only one input, namely the generator rotor speed. The same techniques presented can be applied also for different types of input and for multi-input PSSs. The proposed state-space system identification method can be easily adapted to a multi-input multi-output system. Moreover, different tuning methods can be investigated. In particular, optimal and robust control design [46] would be of particular interest.

Coordinate PSS design and Wide-area control In the proposed work, the PSSs are retuned one at a time based on local measurements. It will be interesting to consider the case of a coordinated design of PSSs. In this case, identifying a multi-input multi-output model is needed. To obtain the model, the system has to be excited in different locations spread around the system and this could be challenging. Moreover, as PSS input, one can consider not only local measurement, but also signals from different sensors in the grid.

Application to HVDC and FACTS Finally, the same system identification methods can be applied for the identification of a power system model for different control devices, such as HVDC and FACTS

References

[1] *AIT Austrian Institute of Technology GmbH*. URL: https://www.ait.ac.at.

[2] ENTSO-E. *Analysis of CE Inter-Area oscillations of 19 and 24 February 2011*. 2011.

[3] ENTSO-E. *Analysis of CE Inter-Area oscillations of 1 December 2016*. 2017.

[4] ENTSO-E. *Oscillation event 03.12.2017*. 2018.

[5] AN Cuk Supriyadi et al. "Adaptive robust PSS to enhance stabilization of interconnected power systems with high renewable energy penetration". In: *Renewable energy* 63 (2014), pp. 767–774.

[6] Arun G Phadke and James S Thorp. *Synchronized phasor measurements and their applications*. Vol. 1. Springer, 2008.

[7] Guoping Liu, Jaime Quintero, and Vaithianathan Mani Venkatasubramanian. "Oscillation monitoring system based on wide area synchrophasors in power systems". In: *2007 iREP symposium-bulk power system dynamics and control-VII. Revitalizing Operational Reliability*. IEEE. 2007, pp. 1–13.

[8] John F Hauer, CJ Demeure, and LL Scharf. "Initial results in Prony analysis of power system response signals". In: *IEEE Transactions on power systems* 5.1 (1990), pp. 80–89.

[9] Daniel Ruiz-Vega, Arturo R Messina, and Mania Pavella. "Online assessment and control of transient oscillations damping". In: *IEEE Transactions on Power Systems* 19.2 (2004), pp. 1038–1047.

[10] Dinesh Shetty and Nagesh Prabhu. "Low frequency oscillation detection in smart power system using refined Prony analysis for optimal allocation of supplementary modulation controller". In: *2019 3rd International Conference on Trends in Electronics and Informatics (ICOEI)*. IEEE. 2019, pp. 418–424.

[11] Naoto Kakimoto et al. "Monitoring of interarea oscillation mode by synchronized phasor measurement". In: *IEEE Transactions on Power Systems* 21.1 (2006), pp. 260–268.

[12] Mariesa L Crow and A Singh. "The matrix pencil for power system modal extraction". In: *IEEE Transactions on Power Systems* 20.1 (2005), pp. 501–502.

[13] Hesen Liu et al. "ARMAX-based transfer function model identification using wide-area measurement for adaptive and coordinated damping control". In: *IEEE Transactions on Smart Grid* 8.3 (2015), pp. 1105–1115.

[14] Hesen Liu et al. "Comparison of MIMO system identification methods for electromechanical oscillation damping estimation". In: *2016 IEEE Power and Energy Society General Meeting (PESGM)*. IEEE. 2016, pp. 1–5.

[15] Yong Liu, Kai Sun, and Yilu Liu. "A measurement-based power system model for dynamic response estimation and instability warning". In: *Electric Power Systems Research* 124 (2015), pp. 1–9.

[16] Rahul Chakraborty, Himanshu Jain, and Gab-Su Seo. "A review of active probing-based system identification techniques with applications in power systems". In: *International Journal of Electrical Power & Energy Systems* 140 (2022), p. 108008.

[17] Junbo Zhang and Hanchen Xu. "Online identification of power system equivalent inertia constant". In: *IEEE Transactions on Industrial Electronics* 64.10 (2017), pp. 8098–8107.

[18] Mauricio Cespedes and Jian Sun. "Impedance modeling and analysis of grid-connected voltage-source converters". In: *IEEE Transactions on Power Electronics* 29.3 (2013), pp. 1254–1261.

[19] John F Hauer et al. "Use of the WECC WAMS in wide-area probing tests for validation of system performance and modeling". In: *IEEE Transactions on Power Systems* 24.1 (2009), pp. 250–257.

[20] Ning Zhou, John W Pierre, and John F Hauer. "Initial results in power system identification from injected probing signals using a subspace method". In: *IEEE Transactions on power systems* 21.3 (2006), pp. 1296–1302.

[21] Sayak Mukherjee, Saman Babaei, and Aranya Chakrabortty. "A measurement-based approach for optimal damping control of the New York state power grid". In: *2018 IEEE Power & Energy Society General Meeting (PESGM)*. IEEE. 2018, pp. 1–5.

[22] Robert Eriksson and Lennart Söder. "Wide-area measurement system-based subspace identification for obtaining linear models to centrally coordinate controllable devices". In: *IEEE Transactions on Power Delivery* 26.2 (2011), pp. 988–997.

[23] Innocent Kamwa and Luc Gerin-Lajoie. "State-space system identification-toward MIMO models for modal analysis and optimization of bulk power systems". In: *IEEE Transactions on Power Systems* 15.1 (2000), pp. 326–335.

[24] Xavier Bombois and Luigi Vanfretti. "PSS performance monitoring and PSS redesign based on system identification techniques". In: (2022).

[25] Peter W Sauer, Mangalore A Pai, and Joe H Chow. *Power system dynamics and stability: with synchrophasor measurement and power system toolbox*. John Wiley & Sons, 2017.

[26] IEEE PES. "Dynamic Models for Turbine-Governors in Power System Studies". In: (2013).

[27] "IEEE Recommended Practice for Excitation System Models for Power System Stability Studies". In: *IEEE Std 421.5-2016 (Revision of IEEE Std 421.5-2005)* (2016).

[28] Michael John Gibbard, Pouyan Pourbeik, and David J Vowles. *Small-signal stability, control and dynamic performance of power systems*. University of Adelaide press, 2015.

[29] Francois Dussaud. *An application of modal analysis in electric power systems to study inter-area oscillations*. 2015.

[30] Lennart Ljung. "System identification". In: *Signal analysis and prediction*. Springer, 1998, pp. 163–173.

[31] Mattia Zorzi. *Lectures on System Identification*. Amazon, 2020.

[32] Michel Verhaegen. "Identification of the deterministic part of MIMO state space models given in innovations form from input-output data". In: *Automatica* 30.1 (1994), pp. 61–74.

[33] Wallace E Larimore. "Canonical variate analysis in identification, filtering, and adaptive control". In: *29th IEEE Conference on Decision and control*. IEEE. 1990, pp. 596–604.

[34] Peter Van Overschee and Bart De Moor. "A unifying theorem for three subspace system identification algorithms". In: *Automatica* 31.12 (1995), pp. 1853–1864.

[35] Lennart Ljung. "System identification toolbox". In: *The Matlab users guide* (1988).

[36] S Joe Qin. "An overview of subspace identification". In: *Computers & chemical engineering* 30.10-12 (2006), pp. 1502–1513.

[37] Alessandro Chiuso and Giorgio Picci. "Consistency analysis of some closed-loop subspace identification methods". In: *Automatica* 41.3 (2005), pp. 377–391.

[38] Alessandro Chiuso. "On the relation between CCA and predictor-based subspace identification". In: *IEEE Transactions on Automatic Control* 52.10 (2007), pp. 1795–1812.

[39] Ivo Houtzager, Jan-Willem van Wingerden, and Michel Verhaegen. "VARMAX-based closed-loop subspace model identification". In: *Proceedings of the 48h IEEE Conference on Decision and Control (CDC) held jointly with 2009 28th Chinese Control Conference*. IEEE. 2009, pp. 3370–3375.

[40] Alessandro Chiuso. "The role of vector autoregressive modeling in predictor-based subspace identification". In: *Automatica* 43.6 (2007), pp. 1034–1048.

[41] Prabha S Kundur and Om P Malik. *Power system stability and control*. McGraw-Hill Education, 2022.

[42] Peter W Sauer, MA Pai, and Joe H Chow. "Power system toolbox". In: (2017).

[43] F Luis Pagola, Ignacio J Perez-Arriaga, and George C Verghese. "On sensitivities, residues and participations: applications to oscillatory stability analysis and control". In: *IEEE Transactions on Power Systems* 4.1 (1989), pp. 278–285.

[44] Abhinav Kumar Singh, Bikash C Pal, et al. "Report on the 68-bus, 16-machine, 5-area system". In: *IEEE PES Task Force on Benchmark Systems for Stability Controls. Ver* 3 (2013).

[45] Texas A&M University Engineering. *Electric Grid Test Case Repository*. URL: `https://electricgrids.engr.tamu.edu/` (visited on 10/17/2022).

[46] Bikash Pal and Balarko Chaudhuri. *Robust control in power systems*. Springer Science & Business Media, 2006.

Acknowledgments

I would like to thank the Austrian Institute of Technology (AIT) that welcomed me and gave me the opportunity to carry out the work presented in this thesis. In a special way, a big thank you goes to my supervisor Catalin Gavriluta for the immense support. Also, I would like to thank Adolfo Anta for his valuable advice.

I also want to thank OPAL-RT Germany, especially Ravinder Venugopal for offering me the opportunity to validate the proposed methods using Hypersim. Also, a big thank you to Cory Paquet-Clouston for his quick and on-point technical support.